Available online at www.sciencedirect.com

ScienceDirect

Advances in Space Research 74 (2024) 415–436

ADVANCES IN SPACE RESEARCH (a COSPAR publication)

www.elsevier.com/locate/asr

Optimal strategies for the exploration of near-by stars

Johannes Lebert [a,*], Andreas M. Hein [b], Martin Dziura [a]

[a] Technische Universität München, Arcisstraße 21, 80333 München, Germany
[b] Initiative for Interstellar Studies (i4is), 27|29 South Lambeth Road, London SW8 1SZ, United Kingdom

Received 11 August 2023; received in revised form 26 March 2024; accepted 2 April 2024
Available online 16 April 2024

Abstract

In the past decade, the discovery of exoplanets has sparked new interests in the idea of interstellar travel and exploration. Despite various proposals for probe concepts and relevant technologies, there is a lack of extensive literature on viable exploration strategies for journeys beyond a single star system. Such exploration strategies might not only have implications on technology development strategies for achieving interstellar exploration but could also enrich existing models for galactic exploration feeding into solutions of the Fermi Paradox. This article presents optimal strategies for the exploration of a large number of near-by stars, using a dedicated, novel methodology, which sets it apart from existing literature: For the first time, the mission design problem of interstellar exploration is redefined as a bi-objective multi-vehicle open routing problem with profits. It is tackled by an adapted hybrid multi-objective genetic algorithm, which is further improved and modified according to the problem characteristics (e. g. large search space). The overall mission model assumes probes traveling on straight trajectories, utilizing flybys, and maintaining an average velocity of 10% of the speed of light. Surpassing prior research that typically relies on statistical models or restricted star data, the star models are founded on the second Gaia data release (Gaia DR2), which represents the most extensive star catalogue to the date of this study and is employed for the first time in the context of interstellar exploration. The resulting star model contains a maximum of 10,000 stars within a spherical region around Sol, covering a distance of 110 light years.

It is found, that the number of explored stars J_1 scales with mission duration J_2 and probe number m according to $J_1 \sim J_2\, m^{0.66}$, which provides an initial guidance for future interstellar mission design. Furthermore, the routes and selection of stars vary depending on the number of probes used: When conducting missions with a large number of probes, stars in close proximity to the Solar System are given more focus. On the other hand, missions with a small number of probes include more distant stars to facilitate shorter transfers along the route. Based on these findings, the following recommendations for interstellar exploration strategies can be drawn: When energy resources such as fuel reserves are scarce and the exploration mission is not limited to nearby stars, low probe numbers are more efficient. In contrast, high probe numbers enable faster exploration of nearby stars but involve less resource-efficient transfers, making them a suitable option for small, remotely propelled probe concepts. To address crowding effects in high probe number missions, swarm-based probe concepts are recommended based on the scaling law characteristics derived.

Keywords: Interstellar exploration; Interstellar travel; Spaceflight; Multi-target mission; Genetic algorithm; Optimization

1. Introduction

In the recent decade, the increasing number of discovered exoplanets has revived discussions on interstellar travel and exploration. The Breakthrough Starshot program is likely the most well-known example, having been

* Corresponding author.
E-mail address: johannes.lebert@tum.de (J. Lebert).

https://doi.org/10.1016/j.asr.2024.04.003
0273-1177/

launched only a few months before the announcement of an exoplanet detected in the Alpha Centauri system in 2016 (Radford, 2016; European Southern Observatory, 2016). This program involves a gram-scale probe (= probe with a mass on the order of grams), which is accelerated by a laser-driven lightsail to 20% of the speed of light (Parkin, 2018). At that velocity, the probe could reach the Alpha Centauri system in 20 years. Assuming that the current trends continue and gain more momentum, it is likely that the concept of interstellar travel will become less hypothetical and speculative in the coming decades, particularly for uncrewed probes.

However, numerous challenges need to be overcome for interstellar spaceflight to become a reality, beginning with the design and development of a propulsion system capable of reaching near-relativistic velocities. There is already a range of suitable technologies discussed in the literature (see Long (2012) for an overview). For instance, the aforementioned Breakthrough Starshot concept relies on a laser beam, that exerts a max. force of 520 N to achieve a max. acceleration of 14,900 g on the lightweight sailcraft. The overall acceleration process, after which the probe reaches 20% of the speed of light, is planned to last for 9 minutes (Parkin, 2018). Very differently, in Project Daedulus nuclear pulse rockets are employed over a boost period of almost 4 years, generating thrust in the orders of 10^5–10^6N to achieve a coast velocity of 12% of the speed of light (Bond et al., 1978).

According to the different propulsion techniques, the interstellar probe concepts proposed in the literature vary greatly in scale, covering nanoprobes with few grams (Kulkarni et al., 2018) as well as giant spacecraft with a mass of several tons (Forward, 1984) or even thousands of tons (Bond et al., 1978). Such heavy-weighted spacecraft would enable extensive instrumentation for conducting scientific research, with major benefits anticipated in the fields of stellar astrophysics, planetary science, astrobiology, and interstellar medium studies (Crawford, 2009). For example, the 3-ton payload foreseen in Project Longshot (Beals et al., 1988) allows for various scientific investigations already during the journey itself (using particle detectors) and later upon arrival at the target star system. This involves characterizing the star system and the thermal environment of potential planets (using IR imagers and UV telescopes), as well as determining their composition through spectrophotometry. Subject to stricter payload constraints, smaller and lightweight nanoprobes can be equipped with a micro-electromechanical systems (MEMS) – based sensor package including a spectrometer and a small camera (Hein et al., 2017), which at least enable visual imaging of the target star system. Potential impacts of relativistic effects on such imaging systems have been investigated by Zhang and Li (2018): For velocities as envisaged in Breakthrough Starshot (max. 20% of the speed of light), mild relativistic effects are predicted, manifesting in a maximum Doppler factor of 1.2247. Consequently, this could result in either a positive or negative frequency shift of 22%, depending on the direction of relative motion.

Sending the gathered scientific data and images back to Earth poses another challenge, which is discussed by Messerschmitt et al. (2023) in the context of limited mass budgets. For Breakthrough Starshot, Parkin (2020) proposed a 100 W laser as transmitter and a 30 m telescope as the receiver. While this setup would enable significant image and data transfer (estimated raw data rate of 8–50 Gbit/year), aperture and power assumptions exceed current technological capabilities. Conversely, for heavier spacecraft such as Project Daedalus, the development of suitable communication systems was already deemed practicable in the late 1970s (Bond et al., 1978).

There is a number of further technological aspects addressed in literature related to interstellar travel and exploration, such as the potential contribution of artificial intelligence (Hein and Baxter, 2018), replicability (Borgue and Hein, 2021; Stephenson, 1982) and the feasibility of interstellar spaceflight in general (Forward, 1986). Some studies also include roadmaps (Elachi et al., 1996; Gilster, 2004) and propose missions to a single destination, mostly considering regions beyond the heliopause (Zeng et al., 2012) or near-by stars such as Tau Ceti (Baumann, 2015), the Alpha Centauri star system (Hein et al., 2017; Forward, 1985; Cohen et al., 2019) or Barnard's star (Bond et al., 1978). However, there exist only a limited number of studies that develop strategies for exploring a significant amount of star systems or a sequence of systems. Most of them are based on very basic and simple assumptions about the spacecraft type (Cartin, 2013), the star systems (Bjoerk, 2007; Cotta and Morales, 2009) and the optimization technique (Valdes and Freitas, 1980; Forgan et al., 2012; Cotta and Morales, 2009). A range of advanced optimization methods were applied in the context of the Global Trajectory Optimization Competition[1] (GTOC) X, which focused on settling the galaxy. This includes concurrent tree search (Izzo et al., 2019), breadth-first search algorithms (Zhang et al., 2019), or a combination of different techniques, such as differential evolution and Ant Colony Optimization (Luo et al., 2019).

However, there is no further analysis of how probe technology and mission architecture impact the exploration strategy. Star systems are often assumed to have a simple spatial distribution and are not classified according to their properties such as the likelihood of hosting planets, rather than using actual observation data. This article seeks to expand on previous work by employing current knowledge of nearby star systems and sophisticated optimization algorithms to develop new interstellar exploration strategies using a dedicated, novel methodology, which sets it apart from existing literature: The novel methodology comprises the classification of interstellar exploration as an optimiza-

[1] The Global Trajectory Optimization Competition (GTOC) is a recurring event, occurring approximately every 1–2 years, that challenges the global research community with trajectory design problems.

tion problem, which has not done before in that context. Furthermore, unlike earlier research that relied on simplistic star models or limited data, this study utilizes the Gaia Data Release 2 (Gaia DR2) to construct a star model of the solar neighborhood. This application of Gaia DR2, the most extensive star catalogue available at the time of this study,[2] represents a pioneering step in the field of interstellar exploration. Ultimately, an optimization algorithm is employed to solve the problem, based on a well-established method and customized for the specific nature of the problem to enhance solution quality.

The article is organized as follows: Chapter 2 describes the used methods, starting with the definition and classification of the problem of exploring various star systems before the optimization models and the optimization algorithm are presented. Chapter 3 covers the main results that are obtained after applying the algorithm to the problem based on the described models. The results are discussed in chapter 4 with respect to their limitations and implications for possible exploration strategies.

The article is based on a Master thesis, which was carried out through a collaboration between the Initiative for Interstellar Studies and the Technical University of Munich. The thesis is available online for further reading (Lebert, 2021), as this article represents a summary of the main ideas and results.

2. Methods: Problem classification, models and optimization algorithm

2.1. Defining interstellar exploration as bi-objective multi-vehicle open routing problem with profits

We consider a (future) scenario, where humankind is technically capable of launching several probes simultaneously from Earth with the aim of exploring various star systems in the solar neighborhood. Each probe is assigned one or more star systems, which will be explored sequentially, representing a stellar route. The focus is on the selection of suitable star systems, along with the number of probes, as these factors are essential for designing a suitable mission architecture.

In this section, the problem of the exploration of various star systems is reduced to its minimum set of variables, which are then used to classify and define the considered problem.

The classification and abstraction of the problem provide access to a large pool of potential optimization methods. By contrast, there exists only limited research on advanced optimization methods specifically applied to interstellar exploration, encompassing advanced methods and algorithms for optimizing interstellar missions.

[2] Note that there is already an updated Data Release (Gaia DR3), which was not available yet at the time of this study.

2.1.1. Problem variables and parameters

Given the high number of parameters, the problem cannot be modeled in its entire complexity. Therefore, the minimal set of parameters to describe the problem of interstellar exploration is identified. From a technical perspective, the parameters involved with interstellar exploration can be subdivided into three groups, which are probe concept and technology (e. g. thrust, probe mass, probe velocity), mission architecture and design (e. g. probe number, star selection, travel time), and star system characteristics (e. g. star location, luminosity). In our considered minimal set of parameters, each group is represented by at least one parameter. For instance, from the parameter group of probe concept and technology, we selected the average velocity of the probe, as it contains implicitly other parameters such as acceleration or deceleration characteristics and cruise velocity of the probe. Other parameters such as probe mass are not included, which entails the advantage that the results are valid for various probe concepts.

Fig. 1 shows the considered set of parameters, each parameter is colored according to its foreseen role within the optimization context. The arrows indicate the impact of the parameters, e. g. the star sequence determines both the mission duration and the mission return. As represented by the different colors, there are three types of parameters in terms of optimization:

- Input parameters (orange): Parameters, that must be provided externally
  - o Average velocity: The average travel velocity of the probe
  - o Star data: All information on the stars, e. g. star locations
  - o Available probe number: The number of probes which can be deployed for fulfilling the mission

- Objectives (blue): Variables, that are considered as optimization goals
  - o Mission duration: Duration of the entire mission
  - o Mission return: Sum of rewards earned during the mission

- Decision variable (green): Variable, that is determined by the optimization algorithm by solving the problem for the selected objectives
  - o Star sequence: Selection and order of stars that are explored by the probes

2.1.2. Optimization problem class identification

From an abstract perspective, the task consists of selecting subsets of locations with assigned rewards s_i and organizing them into routes (as depicted in Fig. 2), with the objective of maximizing the total reward while minimizing the time required to complete the route.

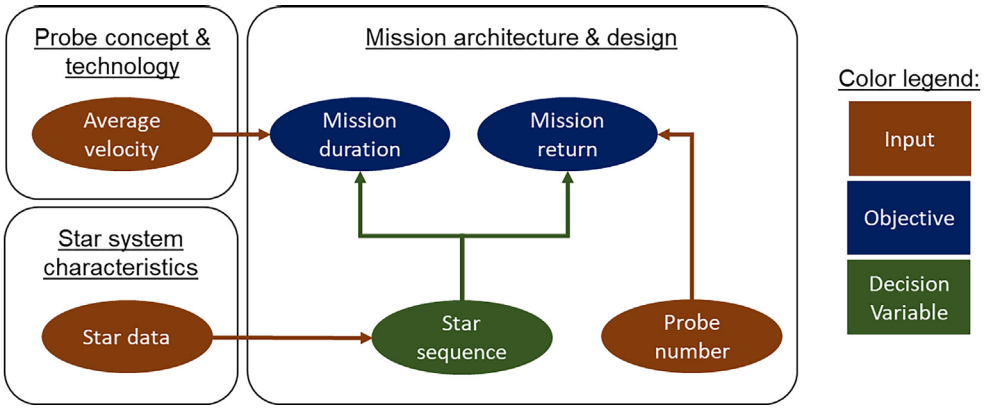

Fig. 1. Parameters considered within the optimization context, color scheme according to each element's role in the optimization.

Assuming a single route, the problem is very similar to the Traveling Salesman Problem (TSP) (Davendra, 2010) and specifically to some of its variations (Gutin and Punnen, 2007), e. g. the TSP with profits (Feillet et al., 2005), tourist trip design problem (Gavalas et al., 2014), vehicle routing problem (Pillac et al., 2013; Dantzig and Ramser, 1959) or orienteering problem (Golden et al., 1987). Accounting for moving locations over time would be analogous to the time-dependent TSP (applied in the case of space debris removal by Zhang et al. (2022)) which, for simplicity, is not considered in this study but potentially of interest for future research.

The creation of multiple routes that are traversed concurrently by a fleet of vehicles leads to a slightly different type of problem that closely resembles the team-orienteering problem (Chao et al., 1996; Bederina and Hifi, 2017). However, there are two main differences that set it apart from the aforementioned problems, despite their apparent similarities:

- Most classical approaches use duration as a constraint representing a time budget, rather than as an objective, resulting in a single-objective problem (e. g. orienteering problem). This means that two routes with the same profit but different durations are equally valued if both are completed within the given time budget. However, as the duration of the route is more critical in the exploration context, we consider it as the second objective in addition to the total reward, resulting in a bi-objective problem.
- Unlike many routing problems or orienteering problems, there is no requirement to specify a fixed destination, known as a depot, where each participant or vehicle must end its route. This feature characterizes the problem as an open routing problem, allowing participants or vehicles to conclude their routes at any desired destination.

Based on the explanations provided, the problem can be classified as a **bi-objective multi-vehicle open routing problem with profits.**

2.1.3. Mathematical formulation of the bi-objective multi-vehicle open routing problem with profits

Note that the problem shares many similarities with the one presented by Bederina and Hifi (2017), which is why most of the definitions used here are adopted from that source. The differences between both approaches are stated in Table 1 along with the corresponding equations.

Assume a connected graph $G = (V, E)$ with nodes $V = \{1, \cdots, n\}$ and edges E that connect pairs of nodes i and j. For the considered problem, the nodes and edges represent the stars and the possible transfers between the stars, respectively (see Fig. 3).

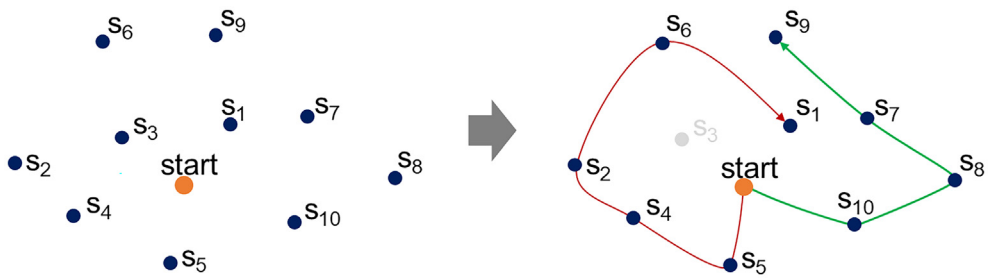

Fig. 2. Problem visualization: From a number of locations with reward s_i, several destinations are picked and organized into routes (route 1 in red, route 2 in green).

Table 1
Problem formulation – differences to original approach and corresponding equations.

Original formulation (Bederina and Hifi, 2017)	Problem as presented here	Affected equations
Start from node 1 (“start depot”)	Start from node 0 (Solar System)	Eq. (8)
Common final target destination n (“arrival depot”)	Open final target choice	Eq. (9)
		Eq. (10)
		Eq. (11)
		Eq. (12)
		Eq. (13)
Optimization w.r.t. overall route duration (sum of route durations)	Optimization w.r.t. maximum route duration of a mission	

Each node i offers a score s_i, that reflects the value of the star system and is added to the total mission return when a probe arrives there. The time required to travel along an edge (i,j) is represented by t_{ij}. It can be calculated from the distance d_{ij} and travel velocity v:

$$\boldsymbol{t_{ij}} = \frac{\boldsymbol{d_{ij}}}{\boldsymbol{v}} \tag{1}$$

Additionally, the binary decision variable x_{ijp} is defined. It takes the value of 1 if the edge (i,j) is traversed on a route p:

$$\boldsymbol{x_{ijp}} = \begin{cases} 1, \ if \ (i, \ j) \in p \\ 0, \ otherwise \end{cases} \tag{2}$$

Analogously, the variable y_{ip} specifies if a star i is element of p, which means if a star is visited or not:

$$\boldsymbol{y_{ip}} = \begin{cases} 1, \ if \ star \ i \in p \\ 0, \ otherwise \end{cases} \tag{3}$$

The variable u_{ip} indicates where a star i is positioned within a route:

$$\boldsymbol{u_{ip}} = \begin{cases} position \ of \ star \ i \ in \ p, \ if \ i \in p \\ 0, \ if \ star \ i \notin p \end{cases} \tag{4}$$

The objective function J_1 is equivalent to the mission return and calculated as follows:

$$\boldsymbol{J_1} = \sum_{p=1}^{m} \sum_{i=1}^{n} \boldsymbol{y_{ip} s_i} \tag{5}$$

In this equation, m denotes number of available probes and n represents the number of stars.

The objective function J_2 is equivalent to the duration of the mission, which is determined by the longest travel time for one route:

$$\boldsymbol{J_2} = \boldsymbol{max}\left(\sum_{i=0}^{n} \sum_{j=1}^{n} \boldsymbol{t_{ij} x_{ijp}} \right), \ \boldsymbol{p} = \{1, \cdots, \boldsymbol{m}\} \tag{6}$$

Hence, if several probes are deployed within one mission, the mission duration is determined by the travel time of that probe that is assigned to the longest route. The overarching goal is to maximize the mission return while minimizing the mission duration.

Mathematically, the optimization problem can then be formulated as follows:

$$\boldsymbol{Z} = \boldsymbol{max}\begin{pmatrix} \boldsymbol{J_1} \\ -\boldsymbol{J_2} \end{pmatrix} \tag{7}$$

Subject to:

$$\sum_{p=1}^{m} \sum_{i=1}^{n} \boldsymbol{x_{0ip}} \leq \boldsymbol{m} \tag{8}$$

$$\sum_{p=1}^{m} \boldsymbol{y_{kp}} \leq 1 \ \forall \ \boldsymbol{k} = 1, \cdots, \boldsymbol{n} \tag{9}$$

$$\sum_{j=1}^{n} \boldsymbol{x_{ijp}} = \boldsymbol{y_{ip}}, \ \boldsymbol{i} = \{1, \cdots, \boldsymbol{n}\} \backslash \{\boldsymbol{w}\}, \ \boldsymbol{p} = \{1, \cdots, \boldsymbol{m}\} \tag{10}$$

$$\sum_{j=0}^{n} \boldsymbol{x_{jip}} = \boldsymbol{y_{ip}}, \ \boldsymbol{i} = \{1, \cdots, \boldsymbol{n}\}, \ \boldsymbol{p} = \{1, \cdots, \boldsymbol{m}\} \tag{11}$$

$$\sum_{i=0}^{n} \sum_{j=1}^{n} \boldsymbol{t_{ij} x_{ijp}} \leq \boldsymbol{T_{max}}, \ \boldsymbol{p} = \{1, \cdots, \boldsymbol{m}\} \tag{12}$$

$$\boldsymbol{u_{ip}} - \boldsymbol{u_{jp}} + 1 \leq \boldsymbol{n}\left(1 - \boldsymbol{x_{ijp}}\right), \ \boldsymbol{i,j} = \{1, \cdots, \boldsymbol{n}\}, \ \boldsymbol{p} = \{1, \cdots, \boldsymbol{m}\} \tag{13}$$

Eq. (8) limits the number of probes launched from the Solar System to a maximum of $\boldsymbol{m}$. Eq. (9) ensures that a star cannot be visited more than once within a mission. Eq. (10) and Eq. (11) check for continuity, which means they guarantee that the number of vehicles entering a star system is equivalent to the number of vehicles exiting it. This effectively rules out the chance of replication. It is pointed out that continuity is not a requirement when a probe arrives at the final star $\boldsymbol{w}$ of its route. To handle this particular situation, $\boldsymbol{w}$ is removed from the input set of $\boldsymbol{i}$ in Eq. (10). This approach differs from the original one where all routes have a common final destination. The maximum total travel time of a probe is limited by the time constraint set in Eq. (12). Eq. (13) prevents the formation of subcycles for a given probe.

2.2. Description of the optimization models

The description of the optimization models concerns mainly the parametrization and definition of the input parameters, which have been introduced above. Given the problem nature, we distinguish between a common probe and mission model, which includes the relevant assumptions on probe and mission architecture, and a star

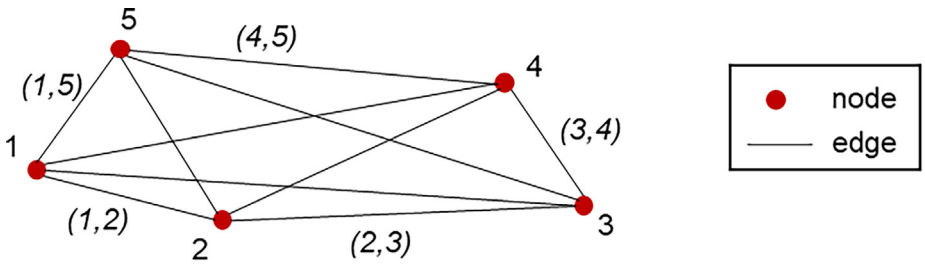

Fig. 3. Sketch of a graph with five nodes and corresponding edges (for better clarity not all edges are numbered).

model, which provides all relevant information on the environment (in particular the star data).

2.2.1. Probe and mission model assumptions

As a first assumption, the mission architecture is restricted to flybys without considering rendezvous. This constraint limits the scientific value of the mission substantially, however, the mission is still valuable, as flybys can be used for the initial reconnaissance of planets (Crawford, 2009). As part of the flybys, the probes are allowed to take arbitrary course corrections, which means that the deflection angle of the trajectory around the target star is not limited. Additionally, the probes cannot replicate or malfunction, ensuring that the number of probes used, denoted by m, remains constant throughout the mission. The probes are assumed to fly at an average velocity $v_{average}$ of 10% of the speed of light which is consistent with literature proposals (Bjoerk, 2007; Valdes and Freitas, 1980). This velocity limit is chosen to enable interstellar travel within a reasonable timeframe, while also ensuring that relativistic effects do not significantly affect the probe's trajectory: With a Lorentz factor of approximately 1.005, the effects of time dilation and length contraction are less than 1% (Kovalevsky and Seidelmann, 2004) and thus negligible in the modeling context. Transfer trajectories between two stars are assumed to occur on rectilinear orbits, as suggested by Fantino et al. (2004).

2.2.2. Star model based on Gaia Data Release 2

To parametrize the star model with the required data, the Gaia Data Release 2 (Gaia DR2) is selected, as it is considered as the most complete and accurate star catalogue at the time of this study. As Gaia DR2 contains spurious data (Lindegren et al., 2018), a filter procedure consisting of several steps is applied to obtain a clean dataset of stars (illustrated in Fig. 4). The filtering follows the approach suggested by Lindegren et al. (2018). It consists of several steps, where sources are first eliminated based on parallax errors and uncertainties in BP and RP fluxes. Further filter steps involve the unit weight error and the flux excess factor. For details, refer to Lindegren et al. (2018).

In Fig. 4, the left plot contains the initial, raw dataset with the nearest 25,000 stars which is obtained from ESA (2018) by using the distance estimates from Bailer-Jones et al. (2018). In the right plot, the filtered dataset is illustrated, containing the 10,000 nearest stars (again based on the distance estimates from Bailer-Jones et al. (2018)) and representing a spherical domain with roughly 110 ly radius around Sol.

For simplicity, the stars are assumed to maintain fixed positions. This assumption can be demonstrated to be applicable for constrained mission durations of 7,000 years by comparing the impact of stellar motion on future star positions with the uncertainties present in current star position estimations: Assuming an orbital velocity with respect to the galactic center of 230 km/s near Sol (Brown, 2016) and considering a timeframe of 7,000 years, the max. positional change due to stellar motion is estimated to be within a few light years. The current stellar position estimations by Bailer-Jones et al. (2018) inherently entail uncertainties which at maximum can be expected in a similar order of magnitude for the considered star set (Lebert, 2021). Hence, incorporating stellar motion in the model would not significantly improve model accuracy, while requiring substantially increased modelling and computational effort. This holds particularly for shorter timeframes (e.g., 1,000 years), where the impact of stellar motion is one order of magnitude smaller compared to the uncertainties in current star estimations.

The model assumption of fixed stars will induce a time constraint in the optimization, which limits the maximum time of a mission to 7,000 years (Eq. (12) in chapter 2.1.3). Note that hypervelocity stars are not considered in the model, given the lack of knowledge and presumable rare occurrence (Boubert et al., 2018).

2.3. Adapted hybrid multi-objective genetic algorithm

2.3.1. Algorithm selection

Due to the large model size (max. 10,000 stars), any algorithm based on enumeration can be ruled out beforehand. Branch and bound methods are not appropriate, as their runtime grows exponentially with the size of the problem (Boyd et al., 2003); at worst their performance is identical to the enumeration approach (Dolgui and Gafarov, 2019). With respect to GTOC X, ESA proposed a concurrent tree search algorithm (Izzo et al., 2019), which we did not consider due to the lack of a suitable growth metric in our case. Population-based algorithms can be useful for

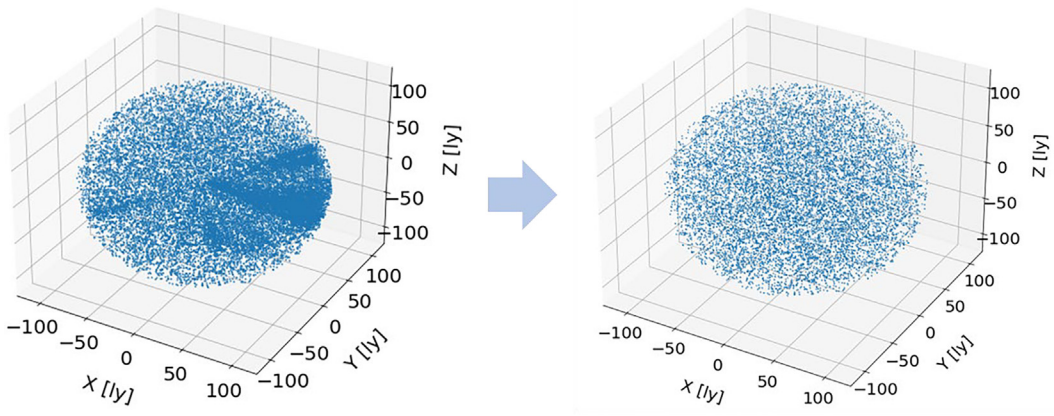

Fig. 4. Left: Selection of nearest 25,000 stars from Gaia DR2 – Right: nearest 10,000 stars after filtering procedure.

analyzing the bi-objectivity of the problem since they provide a set of solutions (Pareto front), instead of a single solution. For instance, Tan et al. (2023) utilize a multi-objective genetic algorithm for designing global navigation satellite system reflectometry missions in low Earth orbit. Considering traditional orienteering problems which are solved with population-based algorithms, various types are used, e. g. Particle Swarm Optimization (PSO) (Dang et al., 2013), Ant Colony Optimization (ACO) (Liang and Smith, 2006) or genetic algorithms (Bederina and Hifi, 2017). Given its strong similarity to the problem presented here, a hybrid genetic algorithm as proposed by Bederina and Hifi (2017) is ultimately chosen. Any other population-based algorithm, PSO or ACO, might be used alternatively.

2.3.2. Genetic encoding of the problem

Inspired by evolutionary process in nature, the genetic algorithm is based on chromosomes, genes, populations and generations. This requires a genetic encoding of the problem and its terms, as depicted in Fig. 5.

A chromosome represents a potential solution to the given problem, which can be viewed as a proposed mission plan. The chromosome is composed of multiple genes, where each gene represents a sequence of stars that a probe will explore during the mission. A group of chromosomes constitutes a population, which is why a chromosome is also denoted as an individual. Since the population varies over time through an evolutionary process, each population is associated with a particular generation.

2.3.3. Optimization procedure and pseudocode

The implemented algorithm largely adheres to the methodology outlined by Bederina and Hifi (2017) with few adaptions which are explained hereafter. The method, referred to as hybrid multi-objective evolutionary algorithm, merges the idea of the Non-Dominated Sorting Genetic Algorithm (NSGA-II) with a set of local search techniques. The concept and essential operations of the genetic algorithm are shown in Fig. 6.

In the beginning, an initial population is created by randomly assigning unexplored stars to the probes of an individual until either the maximum mission duration T_{max} is exceeded or all stars are allocated to a route. Afterwards, three functions, which build the evolution loop, are executed: The first step is to select parents, which are then utilized to produce offspring. The population is then evolved using these children, creating a new generation which serves as the pool for selecting the next set of parents. As per the previously introduced evolutionary terminology, one iteration of the loop is considered as one generation. The loop is exited either after a predetermined number of generations or earlier if the solution is deemed to have converged. By following the functions of the main loop are explained briefly, for a more detailed explanation please see the corresponding chapter on the algorithm description from Lebert (2021).

2.3.3.1. Selection of parents. The parent selection process involves a tournament procedure (Fig. 7), where individuals are randomly arranged in pairs and evaluated based on two criteria: The Pareto rank and the crowding distance.

The Pareto rank of an individual solution is determined by the number of dominating solutions. Dominating solutions provide either a higher mission return in the same or in a shorter time or the same mission return in a shorter time. The more dominating solutions, the higher the Pareto rank of the considered solution. For instance, individuals with rank 0 are non-dominated and build the Pareto front (see Fig. 8).

The crowding distance serves to promote solutions in less crowded, unexplored regions from the search space. Its idea can be imagined by a cuboid around an individual i, which is confined by the neighboring individuals $i-1$ and $i+1$. The normalized side length of this cuboid is equal to the crowding distance of i.

The pseudocode in Fig. 9 shows the calculation procedure of the crowding distance.

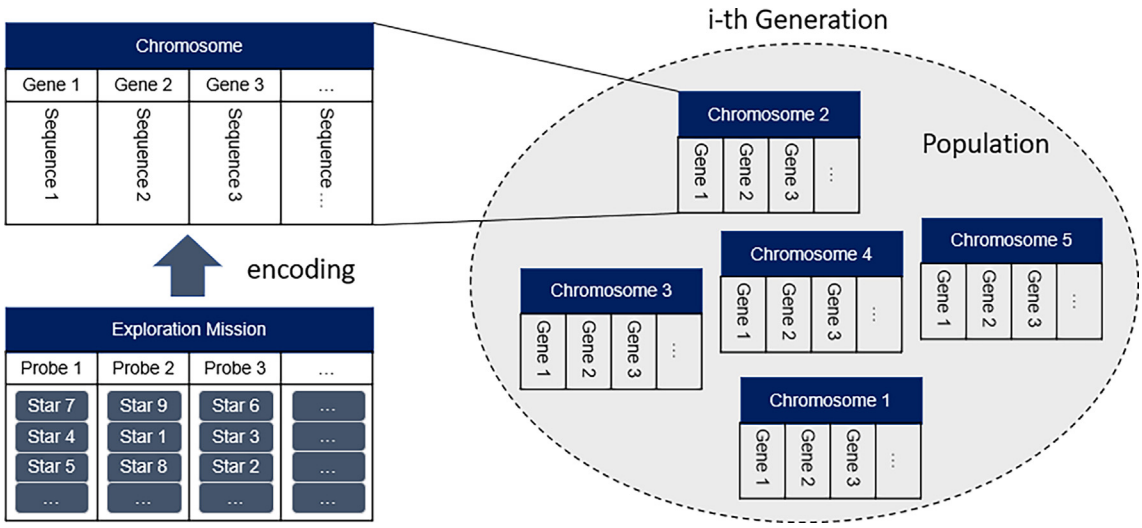

Fig. 5. Evolutionary Algorithm terminology and encoding of exploration mission terms.

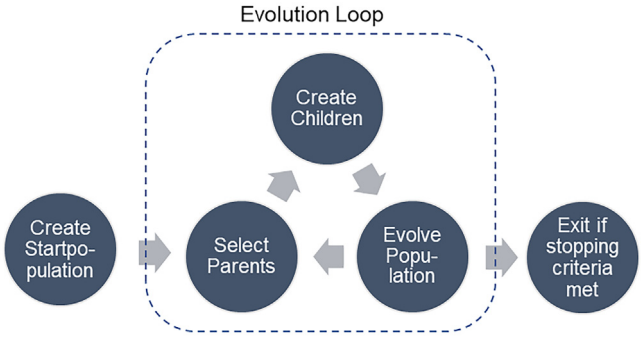

Fig. 6. Overview and main functions of the genetic algorithm.

In step (1), the count of individuals, denoted as l, is determined, constituting the subpopulation I corresponding to a given Pareto rank. In step (2), the crowding distance variable $I[i]_{distance}$ is initialized, with each individual's value being set to 0. Moving to step (3), a loop is initiated to calculate the crowding distance for each objective J_m. Since there are two objectives (mission return and duration), the loop (3) – (7) is executed twice. Step (4) involves sorting individuals in ascending order based on the objective J_m. For instance, if J_m represents mission return, the individual with the lowest return occupies the first position, while the one with the highest return is placed at the end. In step (5), the individuals at the first and end position receive an infinite crowding distance value. This ensures that boundary points are retained for subsequent generations, as individuals with higher crowding distance values are favored during the tournament.

Step (6) initiates another loop, which determines the crowding distance value for the other individuals by measuring the distance to the two neighboring individuals for a given individual $I[i]$ and normalizing the result based on the maximum distance within the considered subpopulation. This normalization method deviates from the original procedure described in Deb et al. (2002) and aims to achieve a more balanced weighting between distances for each objective (see Lebert (2021) for more details). If there is an existing crowding distance value related to previous objectives (e. g. mission duration), the newly calculated

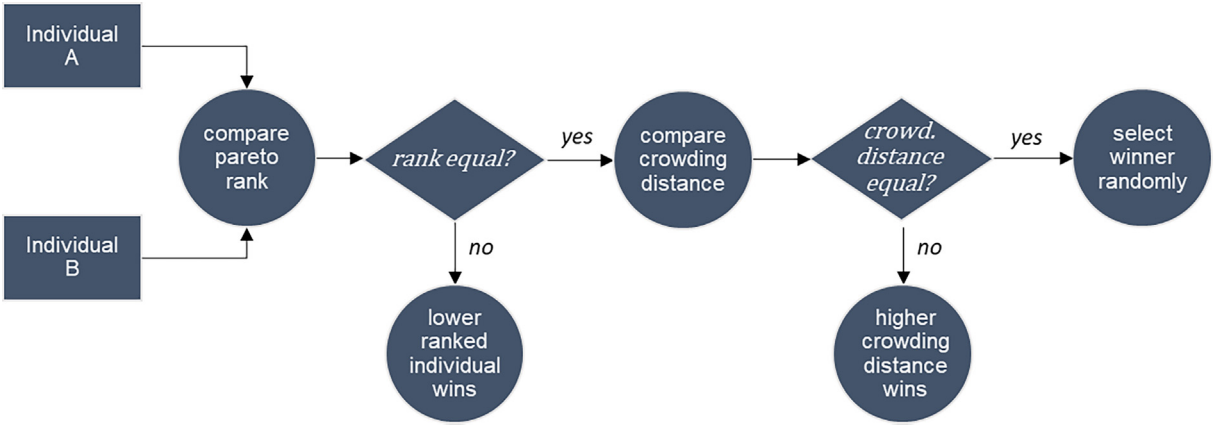

Fig. 7. Overview of the tournament procedure.

value from the different objective (e. g. mission return) is directly added.

The tournament regulation is as follows: Individuals with lower Pareto rank win against individuals with higher Pareto rank. In case of equal Pareto ranks, the individual with the higher crowding distance wins. The winning chromosomes build the parent population and are utilized to create offspring.

2.3.3.2. Generating children. To generate children, two random chromosomes from the parent population replicate their genes and perform a crossover operation (see Fig. 10). Through the crossover operation, the children are able to inherit the best genes from both parents, resulting in each child receiving an additional gene from the other parent. To evaluate the genes, the fitness ratio is utilized, which is simply the ratio of both objectives:

$$\boldsymbol{\sigma} = \frac{\boldsymbol{J}_1}{\boldsymbol{J}_2} \tag{14}$$

The higher the fitness ratio, the more mission return is obtained per time, which is why the gene with the highest fitness ratio is rated as the best one.

After the crossover, some gene entries may appear more than once in the chromosome, which could cause certain stars to be visited multiple times by different probes throughout the mission. To avoid this scenario, the duplicate elements are eliminated from the inherited gene while the crossover gene remains unchanged.

Due to the crossover operation, the children obtain an additional gene, which violates the limit of available probes. To restore the original number of genes, a repair function is implemented, where the worst gene (with the lowest the fitness ratio) is eliminated.

Some of the children that are randomly selected based on the mutation rate r_{mut} will undergo a mutation procedure. Depending on probabilistic rates r_i, different operations are applied, which are partial swapping (r_{swap}), merging the two shortest routes (r_{merge}), splitting the longest route (r_{split}) and shuffling of the routes ($r_{shuffle}$).

After the mutation, all children are checked with respect to their individual route length to account for the time constraint T_{max}. This is done by a cut operation which removes the last stars from routes that violate the time constraint. However, as we found that the solution quality suffers from setting $T_{max} = 7,000\ y$ from the beginning, a dynamic time constraint and stepwise cutting procedure is used: It consists of starting with unconstrained route lengths ($T_{max,g=0} = \infty$) and activating the time constraint in two steps (after g_{cut1} and g_{cut2} generations), where $T_{max,g=g_{cut2}} = 7,000\ y$ to ensure valid solutions at the end of the optimization.

Finally, an improvement procedure is applied to each child in order to balance the travel time between the routes. This is achieved through either filling all the routes, except for the longest one, with unexplored stars until it matches the longest route's travel time, or by trimming each route, except for the shortest one, to the same duration as the shortest route's travel time. The decision between filling or trimming is made based on a probabilistic rate r_{imp_cut}.

The aforementioned process of generating offspring is iterated until the size of the offspring population meets a specified threshold determined by the crossover rate, denoted as r_{cross}. As an example, if $r_{cross} = 1$, then the number of offspring generated will be the same as the size of the original population. Therefore, once the populations are combined, the total population size is doubled, necessitating an additional step to reduce the population size to the desired limit of P_{max}. This is done in the evolving procedure.

2.3.3.3. Evolving population. In the evolving process, the succeeding generation's population is composed sequentially with individuals from the existing population until the maximum population size, P_{max}, is attained. The funda-

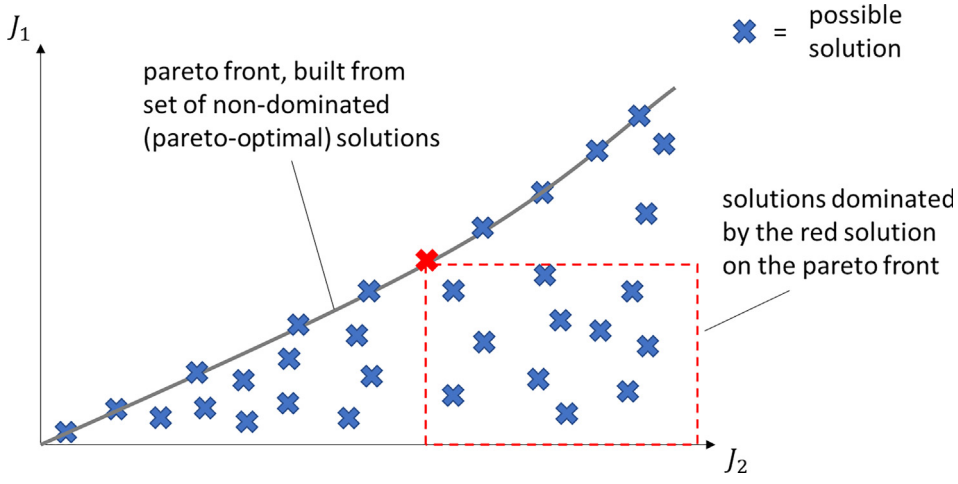

Fig. 8. Pareto front built from non-dominated solutions.

(1) $l = |I|$
(2) for each i, set $I[i]_{distance} = 0$
(3) for each objective J_m
(4) $I = sort(I, J_m)$
(5) $I[1]_{distance} = I[l]_{distance} = \infty$
(6) for $i \in \{2, \ldots, l-1\}$
(7) $I[i]_{distance} = I[i]_{distance} + \frac{J_m(I[i+1]) - J_m(I[i-1])}{\max(J_m(I)) - \min(J_m(I))}$

Fig. 9. Pseudocode for crowding distance calculation (from Deb et al. (2002), adapted).

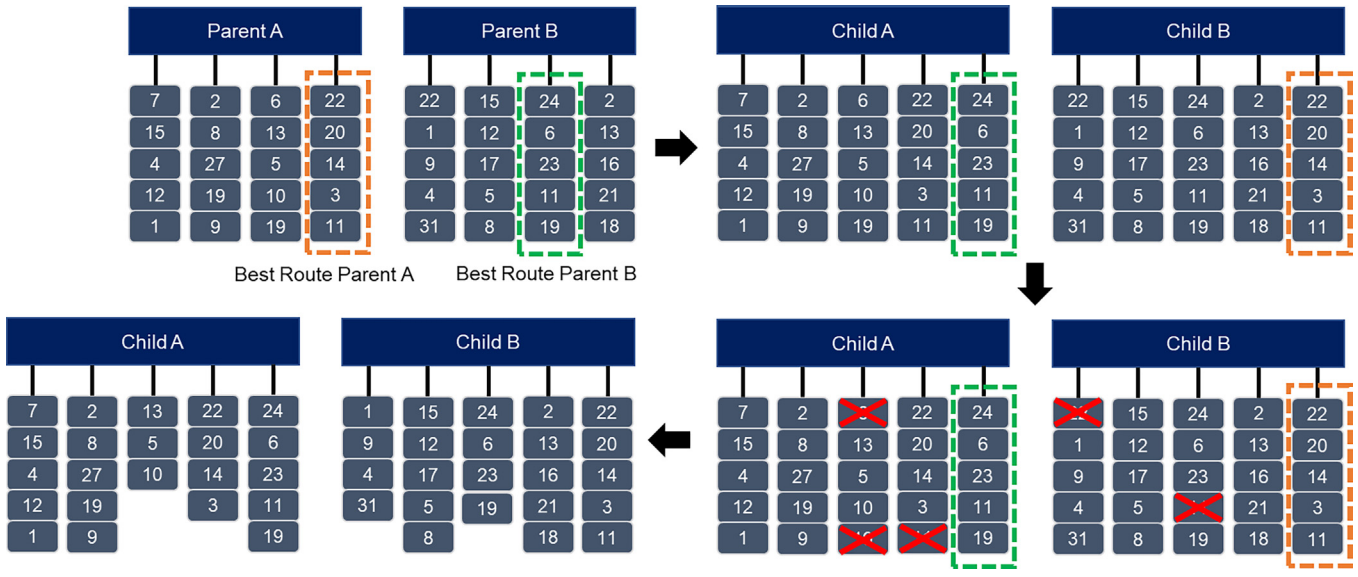

Fig. 10. Replication and crossover operation: Each parent shares its best route (based on fitness ratio σ) with each child; duplicates in the other inherited routes are removed.

mental mechanism, which employs Pareto rank and crowding distance, is depicted in Fig. 11.

Individuals with the lowest Pareto rank (F_1 in Fig. 11) are added first to the evolved population, preceding individuals with higher ranks. When the population limit is nearly approached, individuals with critical rank (F_3 in Fig. 11) are picked depending on the crowding distance. As before, individuals with high crowding distance are prioritized. When the maximum population size is attained, the remaining individuals from the critical rank with lower crowding distance and those with higher Pareto ranks (F_4 upwards in Fig. 11) are discarded.

2.3.3.4. Local search. The local search procedure comprises five different operations, that are executed after a fixed number of generations r_{local_search} throughout the entire population:

A) One-point: A star is randomly selected and moved to a different position along the route.
B) Two-points: Two random stars from the same route exchange their position.
C) Two-opt: A randomly selected segment of the route is reversed.
D) Best insertion: The route is reconstructed based on a nearest neighbor heuristic.
E) Switch from longest to shortest: The final star from the longest route is detached and added to the end of the shortest route.

A)-D) is taken from Bederina and Hifi (2017). E) is an additional feature to the original algorithm and included to address the issue of unbalanced route times within an individual. The idea behind E) is derived from Cotta and Morales (2009), who implemented a similar local search technique called l-opt.

Out of this set, one operation is selected randomly for each individual and then executed on all of its routes. In general, any changes made to the routes through local search operations are retained only if they result in an improved overall solution, which is evaluated using the fitness ratio σ.

The procedure of the local search is illustrated in Fig. 12.

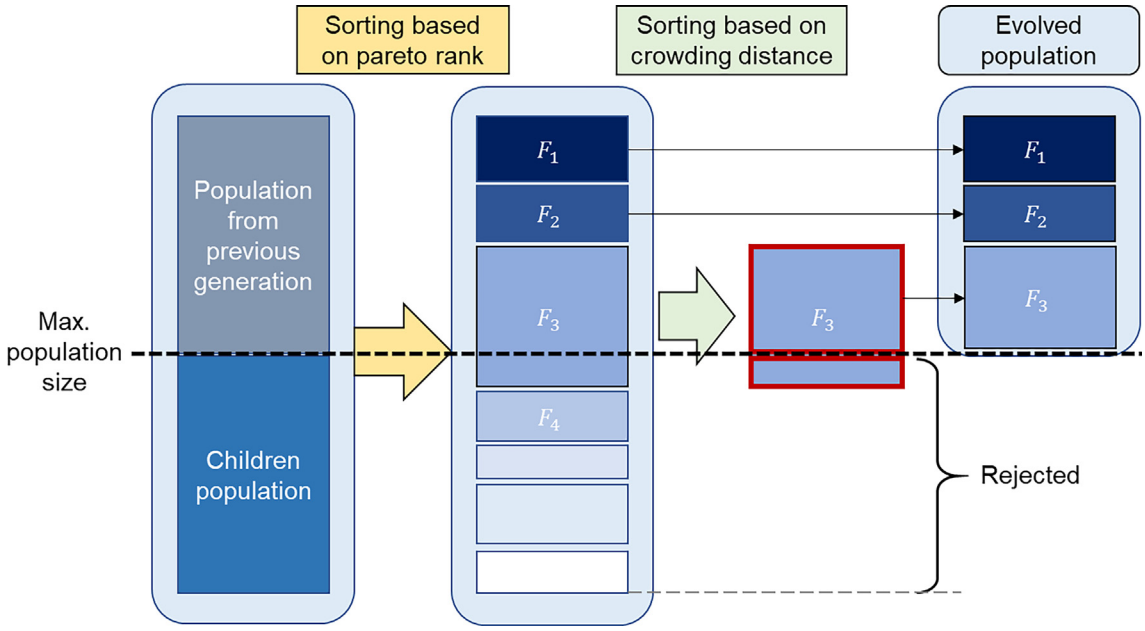

Fig. 11. Evolving procedure based on non-dominated sorting and crowding ranking, F_i refers to a subpopulation of individuals with the same Pareto rank (from Deb et al. (2002), adapted).

2.3.3.5. Stopping criteria. In its original version the algorithm terminates after a fixed number of generations, disregarding the solution's behavior. To reduce the runtime, a convergence check after each loop is developed, based on the average fitness ratio of the current population. The average fitness ratio is determined by the population size P_{max} and the individual fitness ratios σ_i:

$$\boldsymbol{\sigma_{mean}} = \frac{1}{\boldsymbol{P_{max}}} \sum_{i=1}^{\boldsymbol{P_{max}}} \boldsymbol{\sigma_i} \tag{15}$$

The convergence check is realized by monitoring σ_{mean} for 200 generations and smoothing out minor fluctuations with a moving average of size 3. If the ratio between the minimum $\sigma_{mean,min}$ and maximum $\sigma_{mean,max}$ over the given sample is less than 1%, convergence is assumed. To prevent premature convergence resulting from being trapped in local optima, a minimum limit of 300 generations is set. If the convergence criterion is not met, the algorithm will terminate upon completing the maximum generation number g_{max}. Fig. 13 shows the pseudocode of the described optimization algorithm.

3. Model analysis and optimization results

3.1. Preliminary analysis of the spatial star distribution

To obtain a qualitative understanding of the used models, the stars are first analyzed with respect to their spatial coordinates (Fig. 14). Because the model domain is spherical, the analysis is performed using galactic longitude, galactic latitude, and distance as spherical coordinates. As a reference, a uniform distribution curve based on random numbers is provided in orange. Additionally, the distance between each star and its nearest neighbor is examined. Explanations of the approach and figures are given below:

- **Galactic longitude**: Stars are counted based on their longitude, which is divided into 5° intervals ranging from 0 to 360°. The resulting histogram is shown in Fig. 14 upper left.
- **Galactic latitude:** Based on their latitude, stars are assigned to intervals with size 2° (range from −90° to 90°). Unlike longitude, the number of stars in a uniform distribution declines for the latitude values towards the poles. In Fig. 14, lower left, we adopted an approach from Weisstein (n.d.) to model a random distribution of the latitude.
- **Distances to Sol:** The distribution of the distances to Sol is investigated based on a cumulative histogram (Fig. 14 upper right). For each distance value, the corresponding bin in the histogram represents the number of stars that have a distance smaller than or equal to that value. The theoretical curve for a random uniform distribution is given as a reference and has a cubic course because the spheric volume increases with radius according to $V \sim r^3$.
- **Minimum transfer distances:** The histogram in Fig. 14 lower right shows each star's distance to its nearest neighbor. The bin size is 0.25 ly, which means that each bar in the histogram represents the number of stars that have a minimum transfer distance falling within a specific range. For instance, the third bar corresponds to the number of stars that have a transfer distance between 0.5 and 0.75 ly to their nearest neighbor.

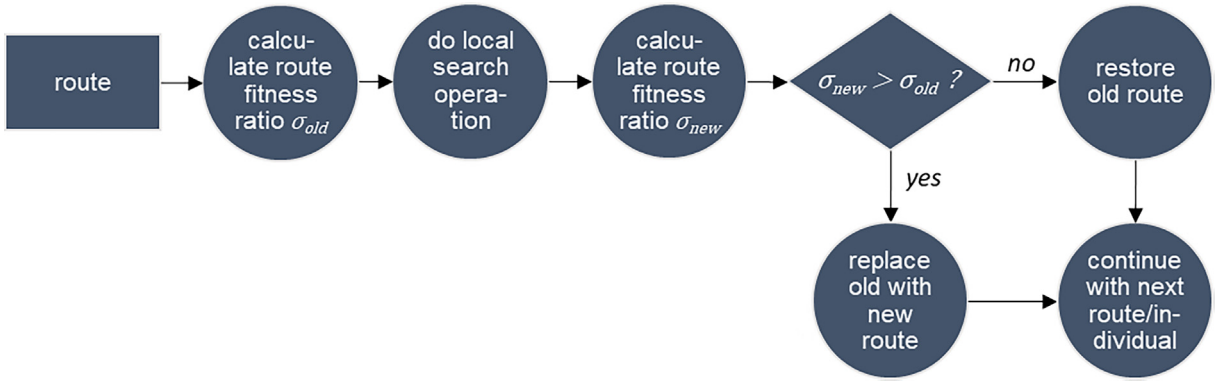

Fig. 12. Illustration of the local search procedure.

On a qualitative level, the plots of the coordinate histograms suggest that the stars are distributed almost uniformly, i. e. without forming clusters. However, apart from the large number of very short transfers smaller than 0.75 ly, the minimum transfer distances (lower right histogram in Fig. 14) appear to follow a Poission distribution. It is assumed, that the peak for the very short minimum transfer distances (stars with distances less than 0.25 ly to their nearest neighbor) is due to the existence of binary or multiple star systems, since in the Gaia release each star source is considered as single star (Lindegren et al., 2018). Under this assumption, over 10% of stars in the model might belong to binary or multiple star systems. In reality, multiple star systems are even more common in the Milky Way, with estimates suggesting that 40–60% of stars form part of multiple systems (Scholz, 2018, p. 109). The discrepancy between the model and the estimations is believed to be due to the restricted resolution of the Gaia observations and the filtering method used: Given that very close binary systems can lead to erroneous results, these stars are removed through the filtering process (see Lindegren et al. (2018) for more details on binaries and multiple star systems in Gaia DR2).

3.2. Results overview for 10,000 stars

For a first analysis of the results, a set of 9 runs[3] is considered and compared. Between each run, the probe number m is doubled, starting with $m = 2$. The star model contains 10,000 stars, hence the maximum mission return J_1 is 10,000, assuming each star provides the same reward $s_i = 1$. See Table 2 for a specification of the used parameters.

Fig. 15 shows the evaluation of the final population for each run with respect to the objectives. The curves represent the estimated Pareto front for the considered problem. Each dot corresponds to an individual and embodies a potential exploration mission.

As one would expect from intuition, the mission return for a given mission duration increases with the probe number. For a certain range (probe number smaller than 256) and given mission duration one finds that the incline of mission return J_1 with probe number m scales roughly with $J_1 \sim m^{0.66}$. This relation has been derived by selecting solutions from the different curves for 2000 years and 4000 years and evaluating them with respect to the mission return. For the considered probe number range, the mission return turned out to increase by an average factor of 1.58, when the probe number is doubled, resulting in:

$$\frac{\boldsymbol{J}_1(2\boldsymbol{m})}{\boldsymbol{J}_1(\boldsymbol{m})} \approx 1.58 \tag{16}$$

Assuming a power relation $J_1 \sim m^x$ with unknown exponent x, one obtains the following expression:

$$\frac{(2\boldsymbol{m})^{\boldsymbol{x}}}{\boldsymbol{m}^{\boldsymbol{x}}} \approx 1.58 \tag{17}$$

Solving for x yields:

$$\boldsymbol{x} \approx 0.66 \tag{18}$$

Furthermore, there appears to be a linear relation between both objectives for a given probe number ($J_1 \sim J_2$). This fits well with the preliminary, qualitative analysis of the spatial star distribution in section 3.1, which revealed an almost uniform star distribution. Note that there are two exceptions from the linear relation: The first one is the curve flattening of run 9 (with 512 probes) as the mission duration approaches longer timeframes, such as beyond 5000 years. This phenomenon is artificially generated by limiting the model to 10,000 stars: In case of high probe number and mission duration (upper right region in the plot), probes are forced to add also stars with less favorable transfers, as most of the available stars have already been explored. In real life, the probes will not run into this issue, as the number of stars is much higher.

The other departure from the linear trend is observed again for high probe number runs, but this time for missions with very short durations. In that region of the curve,

[3] On a modern processor, the calculation time for one single run ranges between several minutes to few hours (depending on the probe number being employed).

input set of n stars with position data and star scores s_i, probe number m, travel speed v

Parameters

Initial time constraint $T_{max,g=0}$	Max. generations g_{max}	Mutation rate r_{mut}
1st cut generation number $g_{cut,1}$	Population size P_{max}	Swap rate r_{swap}
2nd cut generation number $g_{cut,2}$	Crossover rate r_{cross}	Merge rate r_{merge}
1st cut time constraint $T_{max,g=g_{cut,1}}$	Local search rate r_{loc_search}	Shuffle rate $r_{shuffle}$
2nd cut time constraint $T_{max,g=g_{cut,2}}$	Improvement cut rate r_{imp_cut}	

output Population of solutions $P(g)$

begin

$g \leftarrow 0$

$T_{max} \leftarrow T_{max,g=0}$

$P(g) \leftarrow generate\_initial\_population(P_{max}, T_{max})$

while $g < g_{max}$:

  if $g = g_{cut,i}$:

    $T_{max} \leftarrow T_{max,g=g_{cut,i}}$

    $P(g) \leftarrow cut\_routes(P(g), T_{max})$

  end

  $P'(g) \leftarrow P(g)$

  while size($P'(g)$) $<$ $(2\ P_{max}\ r_{cross})$:

    $P_{parent} \leftarrow do\_tournament(P(g))$

    $P_{children} \leftarrow generate\_children(P_{parent})$

    $P'_{children} \leftarrow mutate\_children(P_{children}, T_{max}, r_{mut}, r_{swap}, r_{merge}, r_{shuffle})$

    $P''_{children} \leftarrow improve\_children(P'_{children}, T_{max}, r_{imp\_cut})$

    $P'(g) \leftarrow (P'(g) \cup P''_{children})$

  end

  $P(g) \leftarrow P'(g)$

  $P(g+1) \leftarrow evolve\_population(P(g), P_{max})$

  if $g > 1$ *and* $g\%r_{local\_search} = 0$:

    $P(g+1) \leftarrow do\_local\_search(P(g+1))$

  end

  if $do\_convergence\_check(P(g+1))$=True:

    stop algorithm and return $P(g+1)$

  end

  $g \leftarrow (g+1)$

end

end

Fig. 13. Pseudocode of the adapted hybrid multi-objective genetic algorithm (the "%" symbol in the if-condition for performing the local search denotes the modulo operator).

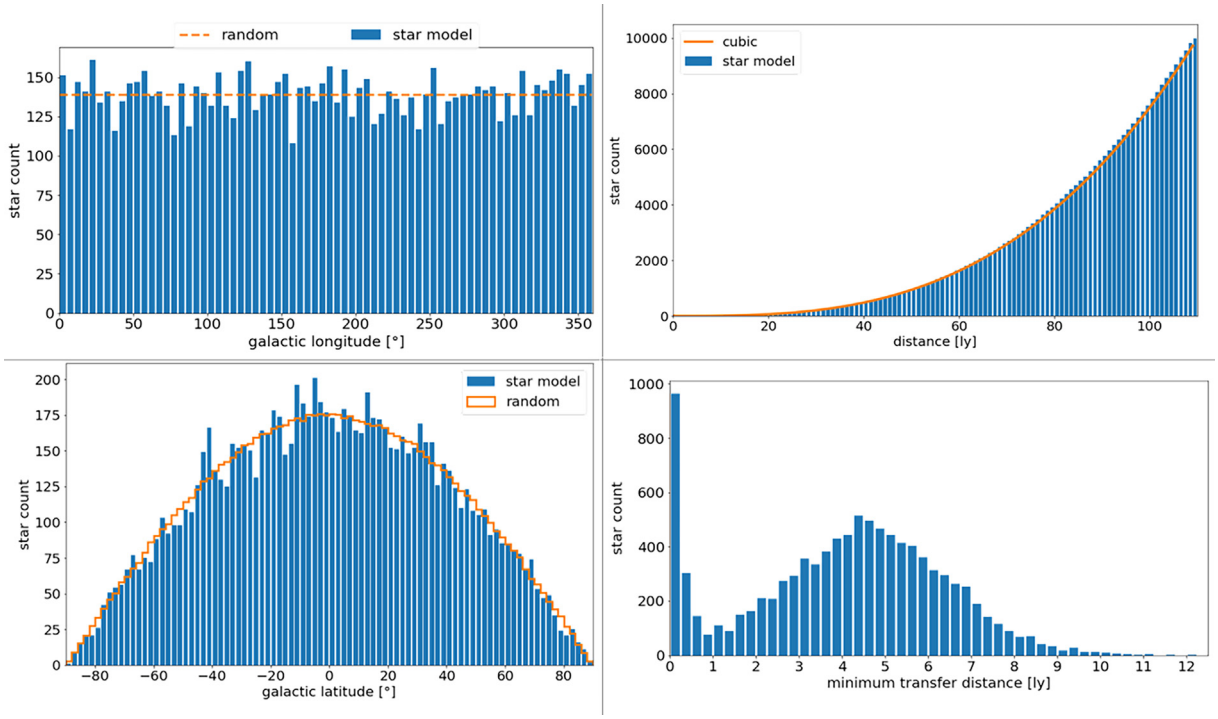

Fig. 14. Qualitative analysis of the spatial star distribution in the 10,000 stars model based on histograms.

Table 2
Specification of input data and algorithm parameter.

Input Data			
Model size	10,000 stars	m	[2, 4, 8, 16, …, 512]
s_i	1	$v_{average}$	0.1c
Algorithm Parameter			
$T_{max,g=0}$	∞	r_{cross}	1
$T_{max,g=g_{cut1}}$	100,000 y	r_{imp_cut}	0.05
$T_{max,g=g_{cut2}}$	7000 y	r_{loc_search}	40
g_{cut1}	100 gen.	r_{mut}	0.4
g_{cut2}	150 gen.	r_{swap}	0.8
g_{max}	1500	r_{merge}	0.5
P_{max}	200	$r_{shuffle}$	0.3

not all available probes are deployed. Hence, the solutions obtained from high probe number runs are converging towards the results from runs with lower probe numbers, as both effectively use the same probe number.

3.3. Scaling law derivation and analysis

The made observations regarding the dependencies of probe number, mission duration and mission return can be condensed into one single equation, denoted as scaling law:

$$J_1 \sim J_2 m^{0.66} \tag{19}$$

Note that this relation holds only in the region of linearity, hence far from approaching the model limits as explained earlier. Furthermore, it is less precise in the case of higher probe numbers.

Assuming a fixed mission duration J_2, the first and second derivative of the mission return J_1 with respect to the probe number are:

$$\frac{d}{dm} J_1 \sim \frac{d}{dm} m^{0.66} = 0.66 m^{-0.34} \tag{20}$$

$$\frac{d^2}{dm^2} J_1 \sim \frac{d^2}{dm^2} m^{0.66} = -0.22 m^{-1.34} \tag{21}$$

As the exponent is negative in both cases, the derivates converge to 0 for high probe numbers. Moreover, the first derivative strictly decreases, since the second derivative is negative irrespective of the probe number. This means, that the increase of mission return with probe number is

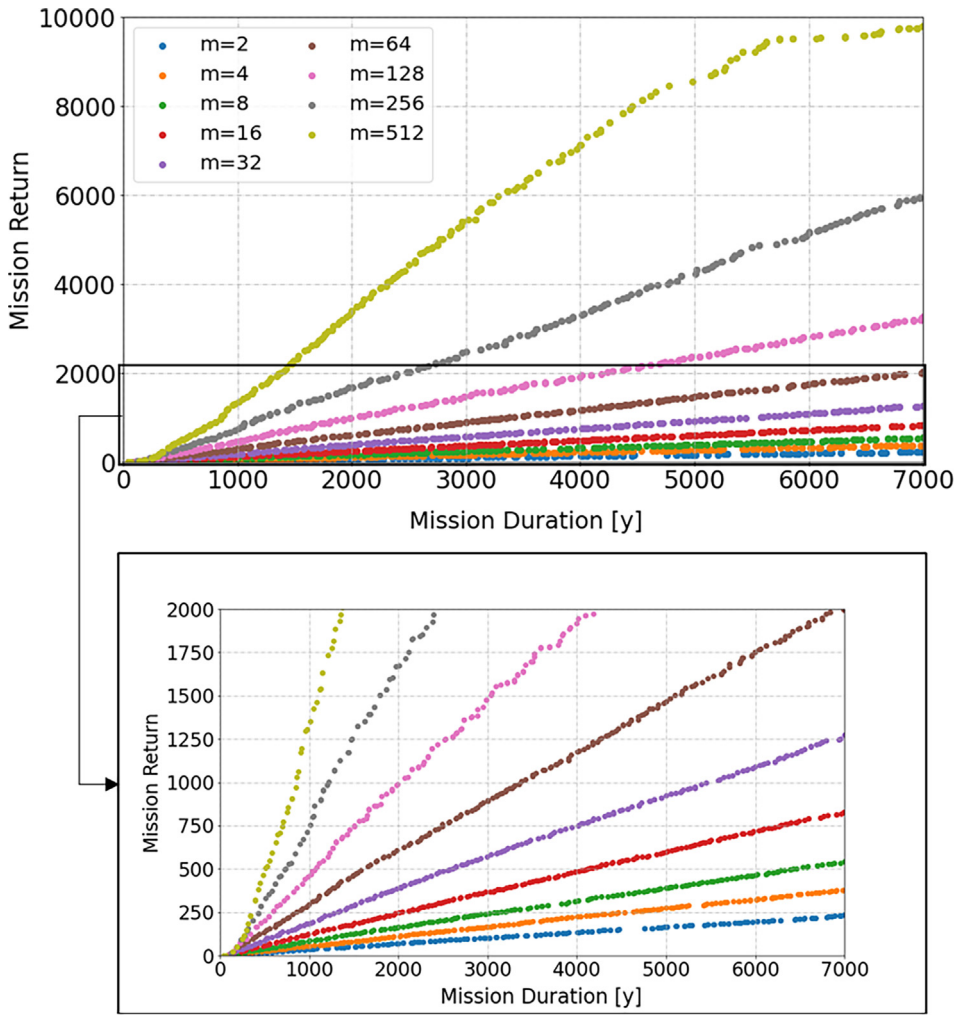

Fig. 15. Final solutions for different probe numbers: each dot represents one solution.

reduced continuously, which is comparable to the concept of diminishing returns: In simple words, diminishing returns refer to a situation where an increase in the input results in a decreasing or reduced increase in the output (Encyclopedia Britannica, n.d.). In the scenario being considered, the probe number represents the input, while the mission return represents the output.

Based on a plot of the first derivative (Fig. 16), this behavior can be concretized. The curve declines strongly for low probe numbers (e. g. less than 10 probes), followed by a slower decrease. From these observations, it can be concluded that in case of very few probes, each additional probe increases the mission return significantly. However, with each additional probe being deployed, this effect diminishes (diminishing returns).

3.4. Star selection and transfer distances analysis

For a more detailed analysis of the algorithm solutions, two different individuals from the final population are selected and investigated with respect to their route structure. Fig. 17 shows two selected individuals, different colors in the lower plots indicate different probes.

As illustrated, the route structure in both solutions is very different, even though they provide roughly the same mission return J_1: The left plot indicates that the optimal mission is built from single-target routes with the probes being sent omnidirectionally towards the nearest stars from Sol. For the considered mission scenario, the explored stars are within 20 light years distance from Sol. The mission in the right plot with 8 probes comprises also more distant stars. As there are fewer probes available, single-target missions are not possible anymore which is why longer routes with appropriate star sequences are constructed.

The described differences in routing structure are also observed when the transfer distances are analyzed in more detail. In Fig. 18, a histogram is shown, which compares the number of transfers with certain distances for two missions with different probe numbers (4 and 64) but similar mission return.

The histogram shows that a small probe number enables shorter transfers. The high probe number scenario, which consists mainly of single target missions (see again

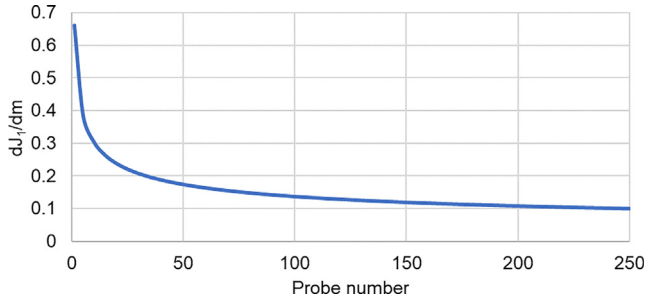

Fig. 16. Plot of the first derivative of the scaling law with respect to probe number.

Fig. 17 left), apparently suffers from the common departure star system (Solar System), which requires longer initial transfers. In contrast, the low probe number case enables more efficient routing due to the chain-like route structure (see again Fig. 17 right). As a result, the benefit of adding probes to the mission decreases for high numbers due to the more distant transfers. This fits well with the observations that are expressed mathematically in the scaling law (chapter 3.3, effect of diminishing returns): For low probe numbers, there are still many nearby stars available, that can be reached by comparably short transfers from Sol. Hence, launching another probe will contribute substantially to the overall mission return without impairing the mission duration.

For very high probe numbers, contrarily, any additional probe is forced to begin its route with a more distant star, as all nearby stars are already assigned to other probes. More distant stars correspond to longer travel times and thus lead to an increase in mission duration. Hence, the gain in mission duration comes at the cost of longer transfers, which makes the deployed probe less efficient.

Notably, the fraction of binary or multiple star systems being explored (indicated by the very short transfers with 0–1 ly in Fig. 18) is significantly higher in the case of lower probe numbers. Therefore, small probe number missions appear to be more appropriate for those systems.

4. Discussion

4.1. Limitations and simplifications

The described methodology is based on various simplifications and limitations. Those, which are considered as most important, are summarized in the following, grouped according to the different methodology elements:

- Assumptions on **probe and mission architecture**: We admit that the probe and mission model is simplistic and represents an ideal case scenario. Simplistic, as the optimization problem only considers the average travel velocity of the probe; other parameters, such as probe mass or relevant subsystems such as communication systems, for example, antennae back to Earth, are not included. Ideal, because we do not question the feasibility of the probe and mission. Based on current technol-

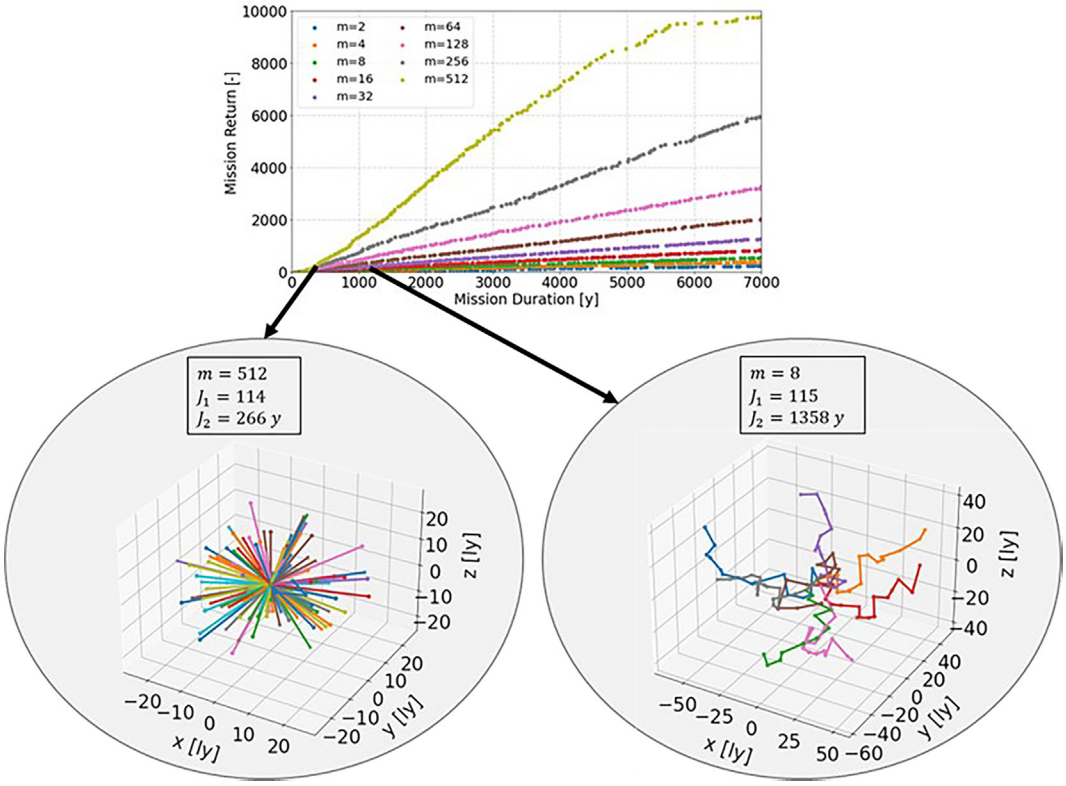

Fig. 17. Route structure for two selected individuals with similar mission return but different probe number.

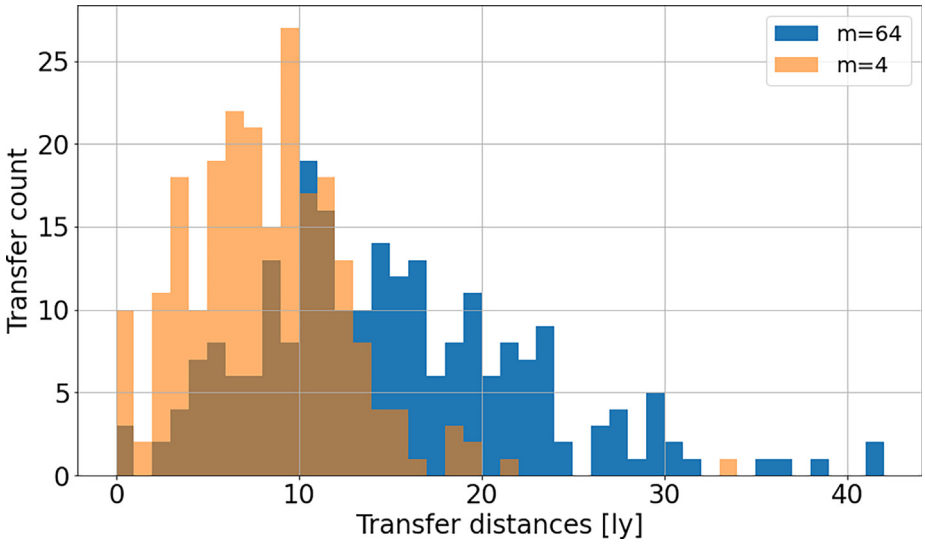

Fig. 18. Distribution of the transfer distances for selected solutions, each bin represents an interval size of 1 ly.

ogy, we cannot expect that probes will operate without failure over timeframes of several hundreds or thousands of years. There is certainly a high degree of autonomy required, ideally paired with self-repairing capabilities, as presented by Moon et al. (2016): They demonstrated high-temperature based self-healing of space electronics damaged by ionizing radiation or hot carrier effects to extend spacecraft lifetime. For future, more realistic studies, one could also incorporate a failure probability per light year travelled (as done by Cartin (2013)), to account for probe failures.

Another significant simplification is the assumption of straight-lined transfers without limiting the angle between two subsequent transfer trajectories. At the considered velocities, however, the possible deflection angles during flybys are limited (for instance, see Moir and Barr (2005)), again raising concerns about mission feasibility. Taking that into account, the results span a theoretical solution space, visualized as a cone with the deflection angle as a vertical dimension (see Fig. 19). Assuming a deflection angle of 0°, the solution space collapses to the cone apex, being limited to single-target missions (one probe per star). On the other end, allowing unlimited deflection angles enables multi-target missions with stellar routes as displayed above. The practicability of these multi-target missions is questionable. They probably require a deceleration phase upon approaching a star (e. g. by means of photogravitational assists as suggested by Heller and Hippke (2017)) before accelerating towards the next star on the route. Further research on this aspect is certainly needed, with the methodology presented here serving as a potential starting point.

- Assumptions on **star model**: Being based on Gaia DR2, the star model is aimed to represent a realistic approximation of the Solar neighborhood. Besides the known limits of Gaia DR2, the main shortcoming of the model is the omission of stellar motion and gravity. It has been shown that the inclusion of stellar motion would not significantly enhance the accuracy of star positions in the model, as its impact is similar to or smaller than that of the current star distance estimations. Consequently, in light of the overarching objective of this study (exploring trends and variations in strategies rather than precise mission planning), this simplification is expected to have no effect on the reliability of the presented findings. However, both stellar motion and gravity could be considered for a more realistic trajectory design, which allows the spacecrafts to perform trajectory corrections or gain velocity e. g. through slingshot maneuvers (Forgan et al., 2012) or photogravitational assists (Heller and Hippke, 2017; Heller et al., 2017). This would also affect the optimal star sequence, e. g. by taking into account whether a star system can be used for maneuvering beside its scientific value. The scientific value is another aspect, which has not been included yet in the model, as all stars are assumed to provide the same reward. For further model refinement, a stellar metric is proposed by Lebert (2021), which assigns each star system a different reward (“stellar score”), taking different aspects into account such as the probability of hosting habitable planets.
- Limitations of the **algorithm**: Due to its metaheuristic nature the used algorithm does not guarantee to find the global optimum. This issue has been encountered with a test model. For a test run with 4 probes, the deviation between the known global optimum and algorithmic solution was found to be about 10%.

A second source which supports the reliability of the results is provided by Cartin (2013), who derived a similar scaling law: Disregarding the influence of the velocity and focusing on the objectives of our study, his

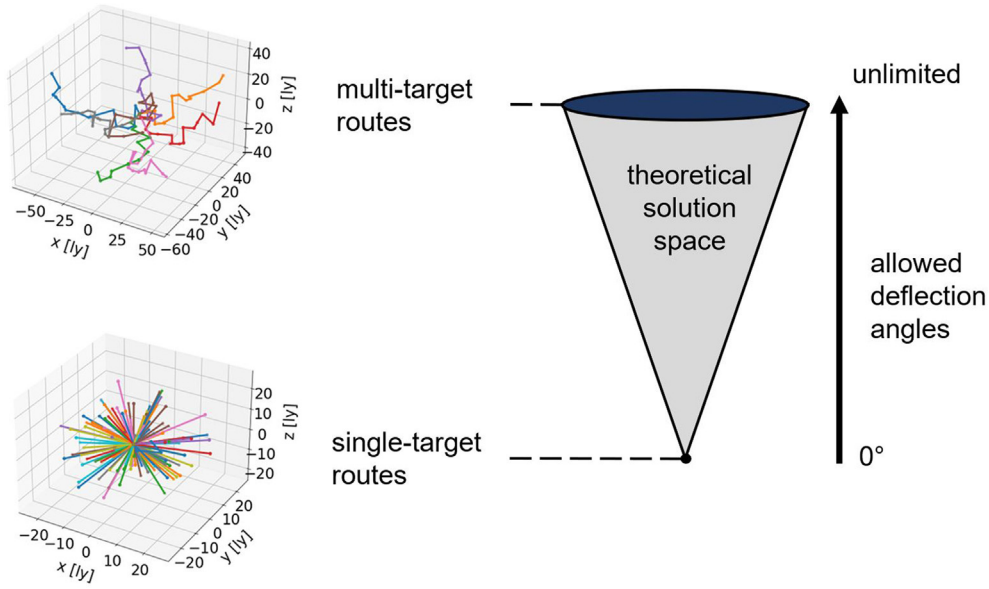

Fig. 19. Theoretical solution space spanned by the results.

scaling law can be rewritten as $J_1 \sim J_2\ m^{0.8}$. Compared to the findings presented here, there is a deviation of approximately 20–30% in the growth factor, thus validating the general trend of the results.

Given these limitations, it is emphasized that the derived results need to be considered rather as trends or tendencies instead of exact solutions.

4.2. Implications for algorithmic and optimization procedure

As a side result, one remarkable observation on the optimization procedure has been made: As there is a limitation of the maximum route length T_{max} required, the routes need to be cut if their length exceeds T_{max} to ensure valid solutions. However, we found that the solution quality can be increased significantly if we initially allow missions with unconstraint route lengths, which has the following reason:

The first generation is created randomly, which leads to very poor routes (long mission duration with few stars explored). With an active time constraint T_{max} the routes have to be cut substantially, which removes many stars that are not shared with subsequent generations. By means of what we refer to as initial relaxation of the time constraint, the routes are not cut in the beginning. Therefore, subsequent generations have access to a maximum number of stars, which allows them to identify better routes due to the enlarged search space. If the time constraint is then activated at a later point in the optimization procedure, the cutting process removes a lower number of stars, as the routes are already partially optimized.

This approach can be useful in various applications and problems which are characterized by a large search space that is significantly confined through an optimization constraint.

4.3. Implications for exploration strategies

Regarding the exploration strategies, various observations have been made concerning the impact of the probe number. Its implications on exploration strategies are summarized below and illustrated in Fig. 20:

- When the mission's objective is to explore many stars close to the Solar System, a larger number of probes is advantageous. Furthermore, the use of a higher number of probes allows for greater customization of scientific instrumentation and equipment for each target star in single-target missions, resulting in a higher scientific return.
- If the probe number is restricted (e. g. in case of high production costs), more distant stars should be considered to increase routing efficiency. However, it should be noted that decreasing the probe number results in a considerable rise in mission duration.
- Overall, missions with low probe numbers enable shorter travel distances to achieve a desired mission return. This should be taken into account in situations where fuel costs are a concern: As the required transfer distance per explored star is lower in that case, deploying fewer probes may be more cost-effective in terms of fuel consumption.
- Exploration missions targeting binary or multiple star systems may benefit from using a lower number of probes.

Finally, a scaling law was derived, which describes the relation between mission return, mission duration and

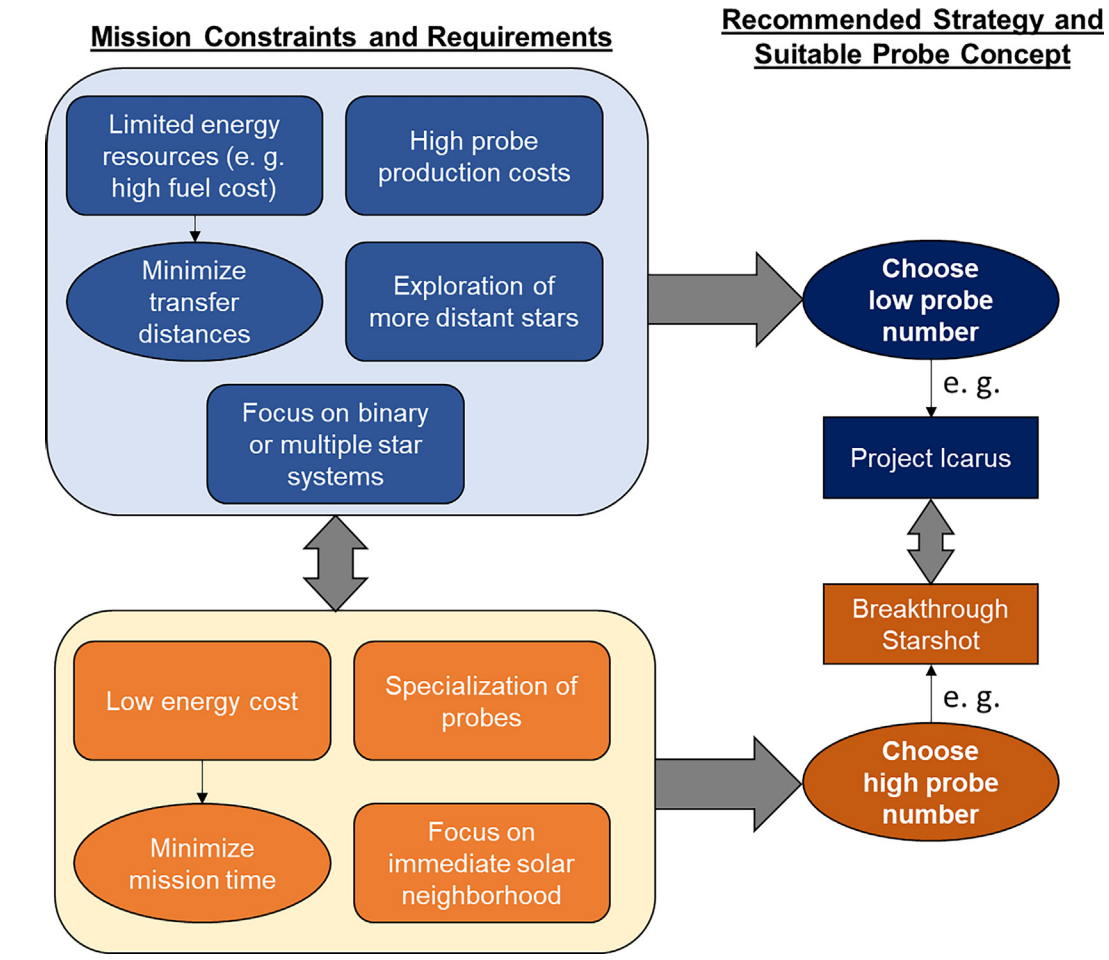

Fig. 20. Strategy recommendations based on mission constraints and requirements including suitable probe concepts from literature.

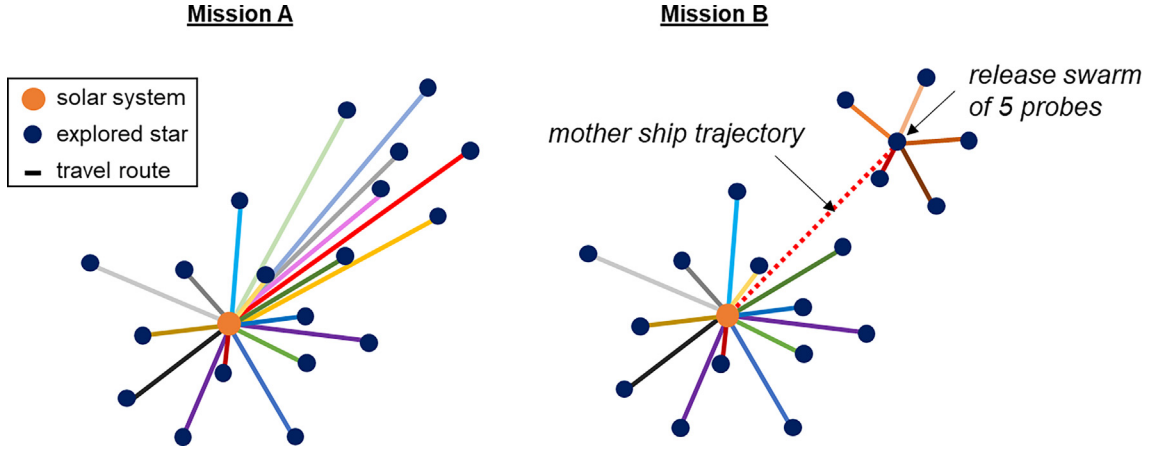

Fig. 21. Benefits of swarm-based probe concepts: By using a mother ship in Mission B, the number of long departure trajectories in Mission A is minimized.

probe number. It revealed that the benefit of deploying additional probes to increase mission return diminishes as the probe number increases. The reason for that behavior is presumably a saturation or crowding effect, as all probes are launched from the Solar System: Due to the common departure site the distance to the nearest star which is still unexplored increases with each probe being launched. This results in large initial transfers if the mission consists of a high number of probes. Besides reducing the probe number, swarm-based mission concepts are an option to

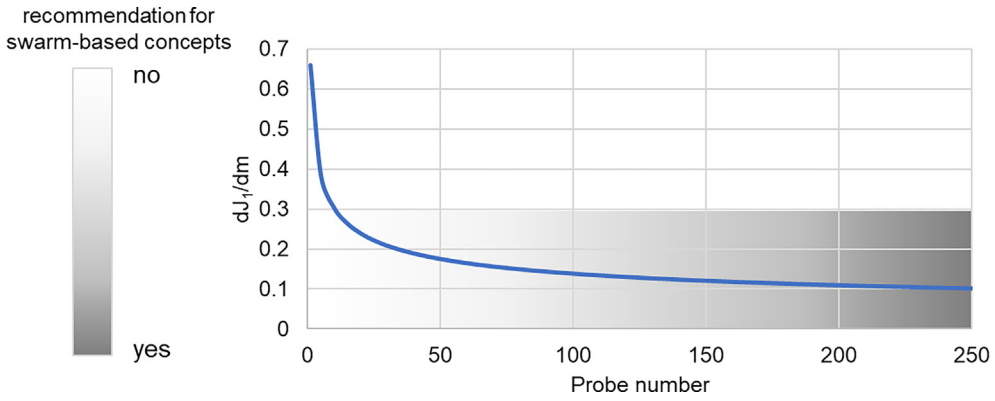

Fig. 22. First derivative of the scaling law with respect to the probe number and recommendation for swarm-based concepts based on qualitative analysis of the scaling law.

circumvent these long departure trajectories: Using a mother ship, a group of smaller probes can be carried to a faraway star or region. Upon arrival, the probes are separated and begin with the actual exploration as visualized in Fig. 21. Probes that are capable of self-replication have a similar effect but might increase the mission duration significantly due to the required replication time.

Based on the described scaling law, one can finally try to derive a qualitative recommendation for swarm-based probe concepts depending on the probe number, as visualized in Fig. 22. According to the indicated trend, for very low probe numbers (say up to a range of 10–20 probes), there is still a substantial increase in mission return with each additional probe being launched. However, one should note that there is a decline in efficiency already from the beginning. For a higher number of probes (say 20–100 upwards) swarm-based concepts should definitely be taken into consideration.

5. Conclusions

This article presented optimal strategies for interstellar exploration missions for nearby stars, using a dedicated methodology. Based on a minimum set of parameters, the design of interstellar exploration missions was defined as a bi-objective multi-vehicle open routing problem. The problem was addressed by a hybrid multi-objective genetic algorithm. The underlying star models use data from Gaia DR2 and include a max. number of 10,000 stars.

Regarding the model and optimization procedures, the following key findings can be inferred from the results: Based on a qualitative analysis, stars in the Solar neighborhood (up to 110 ly distance) appear to exhibit a uniform spatial distribution, however, due to the existence of binary or multiple star systems they are not equally spaced. The technique of initially relaxing the time constraint to enhance the algorithm's performance can be applied in similar structured optimization problems (extensive search space restricted by external constraints).

Regarding potential exploration strategies, the number of probes has significant implications: Deploying a large number of probes is advantageous for missions that focus on exploring the closest stars in Solar vicinity. Another advantage is that using a higher number of probes allows for greater specialization. In general, high probe numbers can reduce mission duration substantially, as indicated by the derived relationship between probe number and optimization objectives. Such missions are most appropriate for utilizing small and lightweight probes where the energy source of the propulsion system is remote (e.g. laser beaming infrastructure), such as proposed in the Breakthrough Starshot project.

On the other hand, a lower number of probes enables a more resource-efficient exploration, mainly because of the shorter transfer distances involved. An additional distinction of low probe number missions is their inclusion of more distant stars and their potential efficiency when targeting binary or multiple star systems. However, missions involving a small number of probes typically require longer routes, which results in longer mission durations. In those cases, more advanced probes might be considered, e. g. with high levels of autonomy. The extended mission duration also necessitates high levels of robustness, and ideally, self-repairing capabilities for the deployed probes. Because of the reduced transfer distances, energy expenses are decreased, thereby enabling the use of large-scale probes equipped with built-in propulsion systems. A probe design appropriate for such missions could be similar to the Daedalus spacecraft or its subsequent projects, such as Project Icarus (Long et al., 2010).

The scaling law obtained from the analysis of the results reveals a behavior closely resembling the principle of diminishing returns. Therefore, a significant increase in mission return due to an increase in probe number can only be expected for low probe numbers. The observed behavior is believed to be caused by a crowding-like effect, which arises when a large number of probes are launched from the Solar System. Swarm-based exploration strategies are recommended to encounter this issue.

Due to the current state of the art with limited research in the area of interstellar exploration, there is a lot of potential for further studies, e. g. in terms of modeling:

For instance, enhancements to the generic probe and mission model can be achieved by incorporating additional variables (such as probe mass), considering rendezvous maneuvers, or taking self-replication capabilities into account. The star model could be extended by including factors such as stellar motion and gravity for a more realistic trajectory design. Furthermore, it would be interesting to incorporate more knowledge on stars and exoplanets by assigning each star a different score (profit) depending on its characteristics (see Lebert (2021) for a suggestion on a stellar metric).

CRediT authorship contribution statement

Johannes Lebert: Conceptualization, Data curation, Formal analysis, Investigation, Methodology, Software, Validation, Visualization, Writing – original draft, Writing – review & editing. **Andreas M. Hein:** Writing – review & editing, Conceptualization, Methodology, Supervision. **Martin Dziura:** Conceptualization, Resources, Methodology, Software, Supervision.

Declaration of competing interest

The authors declare that they have no known competing financial interests or personal relationships that could have appeared to influence the work reported in this paper.

References

Bailer-Jones, C.A.L., Rybizki, J., Fouesneau, M., Mantelet, G., Andrae, R., 2018. Estimating distance from parallaxes. IV. Distances to 1.33 billion stars in Gaia data release 2. Astron. J. 156 (2). https://doi.org/10.3847/1538-3881/aacb21.

Baumann, E., 2015. Swarm-based concepts for resilient autonomous interstellar exploration systems. Insight 18 (1), 34–40. https://doi.org/10.1002/inst.12009.

Beals, K.A., Beaulieu, M., Dembia, F.J., Kerstiens, J., Kramer, D.L., West, J.R., Zito, J.A., 1988. Project Longshot: An Unmanned Probe to Alpha Centauri. US Naval Academy.

Bederina, H., Hifi, M., 2017. A hybrid multi-objective evolutionary algorithm for the team orienteering problem. In: 2017 4th International Conference on Control, Decision and Information Technologies (CoDIT). IEEE, pp. 898–903 https://doi.org/10.1109/CoDIT.2017.8102710.

Bjoerk, R., 2007. Exploring the Galaxy using space probes. Int. J. Astrobiol. 6 (2), 89–93. https://doi.org/10.1017/S1473550407003709.

Bond, A., Martin, A., Buckland, R., Grant, T., Lawton, T., Mattinson, H., Parfitt, J., Parkinson, B., Richards, G., Strong, J., Webb, G., White, T., Wright, P., 1978. Project daedalus – the final report on the BIS starship study. J. Br. Interplanet. Soc.

Borgue, O., Hein, A.M., 2021. Near-term self-replicating probes-a concept design. Acta Astronaut. 187, 546–556. https://doi.org/10.1016/j.actaastro.2021.03.004.

Boubert, D., Guillochon, J., Hawkins, K., Ginsburg, I., Evans, N.W., Strader, J., 2018. Revisiting hypervelocity stars after Gaia DR2. MNRAS 479 (2), 2789–2795. https://doi.org/10.1093/mnras/sty1601.

Boyd, S., Ghosh, A., Magnani, A., 2003. Branch and Bound Methods. Stanford University.

Brown, W.R., 2016. Hypervelocity stars in the Milky Way. Physics Today 69 (6), 52–58. https://doi.org/10.1063/PT.3.3199.

Cartin, D., 2013. Exploration of the local solar neighbourhood I: fixed number of probes. Int. J. Astrobiol. 12 (4), 271–281. https://doi.org/10.1017/S1473550413000098.

Chao, I.-M., Golden, B.L., Wasil, E.A., 1996. The team orienteering problem. Eur. J. Oper. Res. 88 (3), 464–474. https://doi.org/10.1016/0377-2217(94)00289-4.

Cohen, S.A., Swanson, C., Mcgreivy, N., Raja, A., Evans, E., Jandovitz, P., Khodak, M., Pajerj, G., Rognuen, T.D., Thomas, S., Paluszek, M., 2019. Direct fusion drive for interstellar exploration. JBIS – J. Br. Interplanet. Soc. 72 (2), 37–50.

Cotta, C., Morales, A., 2009. A computational analysis of galactic exploration with space probes: implications for the fermi paradox. JBIS – J. Br. Interplanet. Soc. 62 (3), 82–88. https://doi.org/10.48550/arXiv.0907.0345.

Crawford, I.A., 2009. The astronomical, astrobiological and planetary science case for interstellar spaceflight. JBIS – J. Br. Interplanet. Soc. 62, 415–421. https://doi.org/10.48550/arXiv.1008.4893.

Dang, D.C., Guibadj, R.N., Moukrim, A., 2013. An effective PSO-inspired algorithm for the team orienteering problem. Eur. J. Oper. Res. 229 (2), 332–344. https://doi.org/10.1016/j.ejor.2013.02.049.

Dantzig, G.B., Ramser, J.H., 1959. The truck dispatching problem. Manag. Sci. 6 (1), 80–91. https://doi.org/10.1287/mnsc.6.1.80.

Davendra, D., 2010. Traveling Salesman Problem: Theory and Applications. InTech https://doi.org/10.5772/547.

Deb, K., Pratap, A., Agarwal, S., Meyarivan, T.A.M.T., 2002. A fast and elitist multiobjective genetic algorithm: NSGA-II. IEEE Trans. Evol. Comput. 6 (2), 182–197. https://doi.org/10.1109/4235.996017.

Dolgui, A., Gafarov, E., 2019. Can a Branch and Bound algorithm solve all instances of SALBP-1 efficiently? IFAC-PapersOnLine 52 (13), 2788–2791. https://doi.org/10.1016/j.ifacol.2019.11.630.

Elachi, C., Angel, R., Beichman, C., Boss, A., Brown, R., Dressler, A., Dyson, F., Fanson, J., Ftaclas, C., Goad, L., Klein, M., Leger, A., Lillie, C., Peale, S., Peterson, D., Reasenberg, B., Sandler, D., Shao, M., Simon, R., Tenerelli, D., 1996. A road map for the exploration of neighboring planetary systems (ExNPS). JPL Publ., 96–122

Encyclopedia Britannica, n.d. Diminishing returns. Available at: https://www.britannica.com/topic/diminishing-returns

ESA, 2018. Gaia Data Release 2 (Gaia DR2). Available at: https://www.cosmos.esa.int/web/gaia/dr2

European Southern Observatory, 2016. Planet Found in Habitable Zone Around Nearest Star. Pale Red Dot campaign reveals Earth-mass world in orbit around Proxima Centauri. Available at: https://www.eso.org/public/news/eso1629/

Fantino, E., Casotto, S., Izzo, D., 2004. Study on Libration Points of the Sun and the Interstellar Medium for Interstellar Travel. Universitá di Padova/ESA.

Feillet, D., Dejax, P., Gendreau, M., 2005. Traveling salesman problems with profits. Transp. Sci. 39 (2), 188–205. https://doi.org/10.1287/trsc.1030.0079.

Forgan, D.H., Papadogiannakis, S., Kitching, T.D., 2012. The effect of probe dynamics on galactic exploration timescales. arXiv: Popular Physics.

Forward, R.L., 1984. Roundtrip interstellar travel using laser-pushed lightsails. J. Spacecr. Rocket. 21 (2), 187–195. https://doi.org/10.2514/3.8632.

Forward, R.L., 1985. Starwisp-an ultra-light interstellar probe. J. Spacecr. Rocket. 22 (3), 345–350. https://doi.org/10.2514/3.25754.

Forward, R.L., 1986. Feasibility of interstellar travel: a review. Acta Astronaut. 14, 243–252. https://doi.org/10.1016/0094-5765(86)90126-8.

Gavalas, D., Konstantopoulos, C., Mastakas, K., Pantziou, G., 2014. A survey on algorithmic approaches for solving tourist trip design problems. J. Heuristics 20, 291–328. https://doi.org/10.1007/s10732-014-9242-5.

Gilster, P., 2004. Centauri Dreams: Imagining and Planning Interstellar Exploration. Springer, New York, NY.

Golden, B.L., Levy, L., Vohra, R., 1987. The orienteering problem. Naval Res. Log. (NRL) 34 (3), 307–318. https://doi.org/10.1002/1520-6750(198706)34:3%3C307::AID-NAV3220340302%3E3.0.CO;2-D.

Gutin, G., Punnen, A.P., 2007. The Traveling Salesman Problem and Its Variations. Springer https://doi.org/10.1007/b101971.

Hein, A.M., Baxter, S., 2018. Artificial intelligence for interstellar travel. arXiv, preprint arXiv:1811.06526.

Hein, A.M., Long, K.F., Fries, D., Perakis, N., Genovese, A., Zeidler, S., Langer, M., Osborne, R., Swinney, R., Davies, J., Cress, B., Casson, M., Mann, A., Armstrong, R., 2017. The andromeda study: a femto-spacecraft mission to alpha centauri. *arXiv, preprint arXiv:1708.03556*.

Heller, R., Hippke, M., 2017. Deceleration of high-velocity interstellar photon sails into bound orbits at α Centauri. Astrophys. J. Lett. 835 (2), L32. https://doi.org/10.3847/2041-8213/835/2/L32.

Heller, R., Hippke, M., Kervella, P., 2017. Optimized trajectories to the nearest stars using lightweight high-velocity photon sails. Astron. J. 154 (3), 115. https://doi.org/10.3847/1538-3881/aa813f.

Izzo, D., Märtens, M., Öztürk, E., Kisantal, M., Konstantinidis, K., Simoes, L., Yam, C.H., & Hernando-Ayuso, J., 2019. GTOC-X: Our Plan to settle the Galaxy (ESA-ACT).

Kovalevsky, J., Seidelmann, P., 2004. Fundamentals of Astrometry. Cambridge University Press, Cambridge https://doi.org/10.1017/CBO9781139106832.

Kulkarni, N., Lubin, P., Zhang, Q., 2018. Relativistic spacecraft propelled by directed energy. Astron. J. 155 (4), 155. https://doi.org/10.3847/1538-3881/aaafd2.

Lebert, J., 2021. Optimal Strategies for Exploring Near-by Stars. Technische Universität München.

Liang, Y.C., Smith, A.E., 2006. An ant colony approach to the orienteering problem. J. Chin. Inst. Ind. Eng. 23 (5), 403–414. https://doi.org/10.1080/10170660609509336.

Lindegren, L., Hernández, J., Bombrun, A., Klioner, S., Bastian, U., Ramos-Lerate, M., Torres, A.d., Steidelmüller, H., Stephenson, C., Hobbs, D., Lammers, U., Biermann, M., Geyer, R., Hilger, T., Michalik, D., Stampa, U., McMillan, P.J., Castañeda, J., Clotet, M., Vecchiato, A., 2018. Gaia data release 2-the astrometric solution. A & A 616, A2. https://doi.org/10.1051/0004-6361/201832727.

Long, K.F., 2012. Deep Space Propulsion. Springer, New York, NY https://doi.org/10.1007/978-1-4614-0607-5.

Long, K.F., Obousy, R.K., Tziolas, A.C., Mann, A., Osborne, R., Presby, A., Fogg, M., 2010. PROJECT ICARUS: Son of Daedalus, flying closer to another star. arXiv, preprint arXiv:1005.3833.

Luo, Y.Z., Shen, H.X., Huang, A.Y., Zhang, T.J., Zhu, Y.H., Li, Z. ... Yang, Z., 2019. GTOC X: Results and Methods of. National University of Defense Technology and Xi'an Satellite Control Center. In: Proceedings of AAS/AIAA Astrodynamics Specialist Conference.

Messerschmitt, D., Lubin, P., Morrison, I., 2023. Interstellar flyby scientific data downlink design. *arXiv*, preprint arXiv:2306.13550.

Moir, R.W., Barr, W.L., 2005. Analysis of interstellar spacecraft cycling between the Sun and the near stars. J. Br. Interplanet. Soc. 58, 332–341.

Moon, D.I., Park, J.Y., Han, J.W., Jeon, G.J., Kim, J.Y., Moon, J., Choi, Y.K., 2016. Sustainable electronics for nano-spacecraft in deep space missions. In: 2016 IEEE International Electron Devices Meeting (IEDM). IEEE, pp. 31–38 https://doi.org/10.1109/IEDM.2016.7838524.

Parkin, K.L., 2018. The breakthrough starshot system model. Acta Astronaut. 152, 370–384. https://doi.org/10.1016/j.actaastro.2018.08.035.

Parkin, K.L., 2020. A starshot communication downlink. arXiv: Instrum. Meth. Astrophys. https://doi.org/10.48550/arXiv.2005.08940.

Pillac, V., Gendreau, M., Guéret, C., Medaglia, A.L., 2013. A review of dynamic vehicle routing problems. Eur. J. Oper. Res. 225 (1), 1–11. https://doi.org/10.1016/j.ejor.2012.08.015.

Radford, T., 2016. Stephen Hawking and Yuri Milner launch $100m star voyage Available at:. The Guardian https://www.theguardian.com/science/2016/apr/12/stephen-hawking-and-yuri-milner-launch-100m-star-voyage.

Scholz, M., 2018. Die Physik der Sterne. Springer Spektrum Berlin, Heidelberg https://doi.org/10.1007/978-3-662-57801-8.

Stephenson, D.G., 1982. Models of interstellar exploration. Q. J. R. Astron. Soc. 23, 236–251.

Tan, C., Xu, Y., Luo, R., Li, Y., Yuan, C., 2023. Low Earth orbit constellation design using a multi-objective genetic algorithm for GNSS reflectometry missions. Adv. Space Res. 71 (5), 2357–2369. https://doi.org/10.1016/j.asr.2022.10.035.

Valdes, F., Freitas, R.A., 1980. Comparison of reproducing and nonreproducing starprobe strategies for galactic exploration. Br. Interplanet. Soc. J. (Interstellar Stud.) 33, 402–406.

Weisstein, E., n.d. Sphere Point Picking. Available at: https://mathworld.wolfram.com/SpherePointPicking.html

Zeng, X., Alfriend, K.T., Li, J., Vadali, S.R., 2012. Optimal solar sail trajectory analysis for interstellar missions. J. Astronaut. Sci. 59, 502–516. https://doi.org/10.1007/s40295-014-0008-y.

Zhang, B., Li, K., 2018. Relativistic astronomy. Astrophys. J. 854 (2), 123. https://doi.org/10.3847/1538-4357/aaa9b7.

Zhang, N., Zhang, Z., Baoyin, H., 2022. Timeline club: an optimization algorithm for solving multiple debris removal missions of the time-dependent traveling salesman problem model. Astrodynamics 6, 219–234. https://doi.org/10.1007/s42064-021-0107-z.

Zhang, C., Yang, C. H., Zhang, H., Zhang, R. Y., Peng, H., & Gao, Y. , 2019. SETTLER OF THE GALAXY: THE CSU SOLUTION TO GTOCX.